Biogeosciences Discuss., 6, 10381–10446, 2009
www.biogeosciences-discuss.net/6/10381/2009/

Biogeosciences Discussions

This discussion paper is/has been under review for the journal Biogeosciences (BG).
Please refer to the corresponding final paper in BG if available.

Efficiency of small scale carbon mitigation by patch iron fertilization

J. L. Sarmiento[1], R. D. Slater[1], J. Dunne[2], A. Gnanadesikan[2], and M. R. Hiscock[1]

[1]Atmospheric and Oceanic Sciences Program, Princeton University, Princeton, New Jersey, USA
[2]Geophysical Fluid Dynamics Laboratory, NOAA, Princeton, New Jersey, USA

Received: 20 October 2009 – Accepted: 23 October 2009 – Published: 11 November 2009

Correspondence to: J. L. Sarmiento (jls@princeton.edu)

Published by Copernicus Publications on behalf of the European Geosciences Union.

Abstract

While nutrient depletion scenarios have long shown that the high-latitude High Nutrient Low Chlorophyll (HNLC) regions are the most effective for sequestering atmospheric carbon dioxide, recent simulations with prognostic biogeochemical models have suggested that only a fraction of the potential drawdown can be realized. We use a global ocean biogeochemical general circulation model developed at GFDL and Princeton to examine this and related issues. We fertilize two patches in the North and Equatorial Pacific, and two additional patches in the Southern Ocean HNLC region north of the biogeochemical divide and in the Ross Sea south of the biogeochemical divide. We obtain by far the greatest response to iron fertilization at the Ross Sea site. Here the CO_2 remains sequestered on century time-scales and the efficiency of fertilization remains almost constant no matter how frequently iron is applied as long as it is confined to the growing season. The second most efficient site is in the Southern Ocean. Here the biological response to iron fertilization is comparable to the Ross Sea, but the enhanced biological uptake of CO_2 is more spread out in the vertical and thus less effective at leading to removal of CO_2 from the atmosphere. The North Pacific site has lower initial nutrients and thus a lower efficiency. Fertilization of the Equatorial Pacific leads to an expansion of the suboxic zone and a striking increase in denitrification that causes a sharp reduction in overall surface biological export production and CO_2 uptake. The impacts on the oxygen distribution and surface biological export are less prominent at other sites, but nevertheless still a source of concern. The century time scale retention of iron in these models greatly increases the long-term biological response to iron addition as compared with models in which the added iron is rapidly scavenged from the ocean.

BGD

6, 10381–10446, 2009

1 Introduction

The hypothesized link between surface macronutrient concentrations and the air-sea balance of CO_2 has captured the interest of the scientific community ever since a reduction of surface nutrients in the Southern Ocean was first proposed independently by Knox and McElroy (1984), Sarmiento and Toggweiler (1984), and Siegenthaler and Wenk (1984), as a mechanism to explain the observed reduction of atmospheric CO_2 during the ice ages. Building on these and other early box model studies by Joos et al. (1991) and Peng et al. (1991), there have now been a wide range of ocean general circulation model simulations examining the link between macronutrient concentrations at the surface of the ocean and the atmosphere-ocean CO_2 balance (Sarmiento and Orr, 1991; Orr and Sarmiento, 1992; Kurz and Maier-Reimer, 1993; Archer et al., 2000; Matear and Elliott, 2004; Zeebe and Archer, 2005; Marinov et al., 2008; Gnanadesikan and Marinov, 2008). Among the major findings from these large scale macronutrient manipulation simulations are an analysis of how the air-sea CO_2 balance is related to the fraction of total nutrients in the ocean that is remineralized vs. preformed, and the demonstration from regional sensitivity studies that the greatest impact on the global inventory of remineralized nutrients and thus on atmospheric CO_2 occurs when nutrients are depleted in the Southern Ocean High Nutrient Low Chlorophyll (HNLC) region. As regards the second point, Table 1 shows a typical result from nutrient depletion simulations using the KVHISOUTH model from Gnanadesikan et al. (2002), which demonstrates how after 100 yr of nutrient depletion, the Southern Ocean response is about 9 times the average of the other three regions in the North Atlantic, the North Pacific, and the tropical ocean.

The Southern Ocean surface nutrient reduction hypothesis as an explanation for the ice age CO_2 reduction was given a further boost by the suggestion of Martin (1990) that relief of iron limitation by an increased flux of iron-bearing dust might have been the mechanism whereby the macronutrients were reduced during the ice ages. While the ideas about what caused the ice age CO_2 reduction have evolved, including a more

BGD
6, 10381–10446, 2009

recent emphasis on physical mechanisms (e.g., Sigman and Boyle, 2000; Anderson et al., 2009), the evidence in support of the iron limitation hypothesis per se has grown over time based principally on a wide range of mesoscale iron manipulation experiments such as those described by Martin et al. (1994), Coale et al. (1996), Boyd et al. (2000), Gervais et al. (2002), Tsuda et al. (2003), Boyd et al. (2004), Coale et al. (2004), and Hoffmann et al. (2006) (cf. reviews by de Baar et al., 2005; and Boyd, 2007).

The critical importance of the underlying scientific issues regarding our understanding of the linked cycles of carbon, macronutrients, and iron in the ocean have been a strong impetus for continued interest in the hypothesized link between surface nutrient concentration and atmospheric CO_2, and in the iron limitation hypothesis. An additional impetus for study of these hypotheses has been the geoengineering proposal first articulated by Martin et al. (1990a and b) to artificially fertilize the ocean with iron as a way of removing CO_2 from the atmosphere. Studies of this issue have centered primarily on determining: 1) the *efficiency* of the fertilization; 2) the *verifiability* of CO_2 removal from the atmosphere; and 3) the long term *environmental consequences* of the fertilization (cf. Chisholm et al., 2001; Buesseler et al., 2008). This paper is primarily about the underlying scientific issues regarding the efficiency of fertilization, but before proceeding, we note that the potential environmental consequences of extensive iron fertilization alone are sufficient to give serious pause to anyone seriously considering this as an option for CO_2 removal, as discussed by Chisholm et al. (2001), Jin and Gruber (2003), Schiermeier (2003), Shepherd (2009), and Strong et al. (2009) among others; and the verifiability of CO_2 sequestration as analyzed by Gnanadesikan et al. (2003) would be extremely difficult. Despite such findings, the option of carbon mitigation by patch iron fertilization continues to draw interest and thus, if for no other reason, merits serious scientific scrutiny.

The overall efficiency of iron fertilization in removing CO_2 from the atmosphere is defined as the cumulative perturbation atmospheric CO_2 uptake $\Delta\Phi^{CO_2}_{air-sea}$ divided by the cumulative iron addition $\Delta\Phi^{Fe}_{fertilization}$ (see Appendix A for a definition of these terms),

i.e.,

$$R^{\mathrm{C:Fe}}_{\mathrm{overall}} = \frac{\Delta\Phi^{\mathrm{CO_2}}_{\mathrm{air-sea}}}{\Delta\Phi^{\mathrm{Fe}}_{\mathrm{fertilization}}} \quad (1)$$

It is useful to further separate the overall response function into a *physical-chemical efficiency* $e_{\mathrm{phys-chem}}$, defined as the ratio of $\Delta\Phi^{\mathrm{CO_2}}_{\mathrm{air-sea}}$ to $\Delta\Phi^{\mathrm{Org\,C\&CaCO_3}}_{\mathrm{export}}$, which is the cumulative perturbation export of carbon from the surface ocean that results from iron fertilization; and a *biogeochemical response function* $R^{\mathrm{C:Fe}}_{\mathrm{iron\,utilization}}$ defined as the ratio of $\Delta\Phi^{\mathrm{Org\,C\&CaCO_3}}_{\mathrm{export}}$ to $\Delta\Phi^{\mathrm{Fe}}_{\mathrm{fertilization}}$. In equation form, we have that:

$$R^{\mathrm{C:Fe}}_{\mathrm{overall}} = e_{\mathrm{phys-chem}} \cdot R^{\mathrm{C:Fe}}_{\mathrm{iron\,utlization}}, \text{ where}$$

$$e_{\mathrm{phys-chem}} = \frac{\Delta\Phi^{\mathrm{CO_2}}_{\mathrm{air-sea}}}{\Delta\Phi^{\mathrm{Org\,C\&CaCO_3}}_{\mathrm{export}}}, \text{ and} \quad (2)$$

$$R^{\mathrm{C:Fe}}_{\mathrm{iron\,utilization}} = \frac{\Delta\Phi^{\mathrm{Org\,C\&CaCO_3}}_{\mathrm{export}}}{\Delta\Phi^{\mathrm{Fe}}_{\mathrm{fertilization}}}$$

(cf. Jin et al., 2008). The mesoscale iron enrichment experiments referred to earlier have shown that the drawdown in surface dissolved inorganic carbon (DIC) that results from a given iron addition occurs at an average ratio of $R^{\mathrm{C:Fe}}_{\mathrm{DIC\,drawdown}}$= 5600 mol C:mol Fe added (de Baar et al., 2005). This is considerably smaller than the intracellular C:Fe ratios of ~20 000 to 500 000 typically observed in laboratory experiments with oceanic phytoplankton as summarized by Fung et al. (2000) and Sunda (2001), or than the mean C:Fe ratio of 200 000 proposed by Johnson et al. (1997), which are the values typically used in estimating iron demand in geoengineering proposals for iron fertilization. This suggests that most of the iron that is being added to the ocean is not being utilized by phytoplankton, at least on the time-scale of the observations. Results from the iron manipulation experiments thus imply that the iron

BGD
6, 10381–10446, 2009

demand for a given CO_2 removal would be one to two orders of magnitude greater than estimates based on the laboratory measurements (cf. Buesseler and Boyd, 2003). In addition to this problem, there has been only partial success in demonstrating that DIC uptake by iron fertilization actually results in carbon export from the surface ocean. The limited observational period of most experiments seems a likely reason for the failure to observe a significant export flux in many cases (Buesseler et al., 2004; de Baar et al., 2005). For example, in one of the few successful observations of particle fluxes, Bishop et al. (2004) used autonomous floats with optical measurements of the "carbon flux index" to show a large flux of particulate organic carbon at the SOFeX northern patch site beginning only 25 to 45 d after iron addition was initiated. Based on their measurements, Bishop et al. (2004) estimated a C export to Fe added ratio of $R^{\mathrm{C:Fe}}_{\mathrm{iron\,utilization}}$=10 000 to 100 000, which is more in the range of what might be expected from the laboratory experiments.

The problems inherent in short term manipulation experiments have motivated a new series of observational studies at locations within HNLC regions where islands provide a local long-term source of iron. Such studies of natural iron fertilization at the Kerguelen plateau and Crozet Island in the Southern Ocean have detected a large excess particulate organic carbon export in iron fertilized regions relative to that in adjacent non-fertilized regions using the ^{234}Th deficit method. The ratio of the excess C export to Fe supply is estimated to be $R^{\mathrm{C:Fe}}_{\mathrm{iron\,utilization}}$=70 000±46 000 at Kerguelen at the time of observations (Blain et al., 2007). At Crozet Pollard et al. (2009) found that after the chlorophyll peak in the iron fertilized region and in the HNLC region, the mean daily rates of carbon export were similar. However, they calculated different bloom durations for each region by using ^{234}Th/opal ratios to close the silicate budget. The seasonal ratio of excess C export to Fe supply at Crozet was estimated to be 17 200 (5400-60 400) at 100 m and 8600 at 200 m. Estimates based on the seasonal DIC and Fe budgets at Kerguelen give a much higher seasonal mol C:mol Fe ratio of $R^{\mathrm{C:Fe}}_{\mathrm{iron\,utilization}}$=668 000. The reason for the large difference between the Kerguelen and Crozet seasonal estimates of $R^{\mathrm{C:Fe}}_{\mathrm{iron\,utilization}}$ is not understood (e.g., Pollard et al., 2009).

BGD
6, 10381–10446, 2009

Despite the large uncertainties, the natural iron fertilization studies and some of the iron manipulation studies have clearly demonstrated by now that iron fertilization of HNLC regions should eventually give rise to an increased particle export flux. What can we say about the physical-chemical efficiency $e_{\text{phys-chem}}$, i.e., the extent to which the resulting reduction in surface DIC will actually remove CO_2 from the atmosphere? The short time span of the iron manipulation experiments is problematic for verification of the impact of iron fertilization on the air-sea balance of CO_2. A typical air-sea e-folding equilibration time for a 40 m mixed layer is of order 6 months (Sarmiento and Gruber, 2006), as contrasted with the time scale of a few weeks of the experiments. Thus, the air-sea CO_2 flux estimated from the DIC deficit during the fertilization period is only a miniscule part of the carbon budget, an average of 8% of the DIC drawdown per de Baar et al. (2005). The time scale of the natural iron fertilization studies is more suitable, though still not ideal. Estimates of air-sea CO_2 gas flux over a 75-day period during the Crozet Island experiment by Bakker et al. (2007) gave an average uptake of $700\pm600\,\text{mmol}\,\text{m}^{-2}$ inside the fertilized patch vs. $240\pm120\,\text{mmol}\,\text{m}^{-2}$ outside the patch, for a net uptake of $460\pm580\,\text{mmol}\,\text{m}^{-2}$ due to the added iron. Pollard et al. (2009) give a particulate organic carbon (POC) export of $960\,\text{mmol}\,\text{m}^{-2}$ in the patch vs. $290\,\text{mmol}\,\text{m}^{-2}$ outside, for a net of $670\,\text{mmol}\,\text{m}^{-2}$, with no uncertainty reported. The air-sea CO_2 uptake in the Crozet iron fertilized region thus gives a physical-chemical efficiency of $e_{\text{phys-chem}}\sim69\%$, but with quite a large uncertainty. At Kerguelen, we use the 90 d seasonal carbon flux estimates of Jouandet et al. (2008) of $5400\pm1900\,\text{mmol}\,\text{m}^{-2}$ inside the patch vs. $1700\pm400\,\text{mmol}\,\text{m}^{-2}$ outside the patch, and air-sea flux of $28\pm24\,\text{mmol}\,\text{m}^{-2}\,\text{d}^{-1}$ inside the patch and $-2.7\pm2.3\,\text{mmol}\,\text{m}^{-2}\,\text{d}^{-1}$ outside the patch, $\times90\,\text{d}/2$ to account for the whole season, to calculate $e_{\text{phys-chem}}=37\%$, again with a very large uncertainty. However, even the 75 and 90 d time periods over which the air-sea flux was estimated in the natural fertilization studies is insufficient to catch the full equilibration time of the surface DIC perturbation. More importantly, although such studies very likely capture a substantial fraction of the immediate response to iron fertilization, there are other longer term processes that can modify the

BGD
6, 10381–10446, 2009

overall chemical-physical efficiency of the iron fertilization, such as the global backflux of CO_2 that results from reduction of atmospheric CO_2 (cf., Gnanadesikan et al., 2003). This is one of the important places where models can play a crucial role.

Until the addition of explicit representations of ecosystem processes and the iron cycle, macronutrient manipulation studies such as those used in most of the model simulations discussed earlier were the only method whereby the effect of iron fertilization on global biogeochemistry and the air-sea CO_2 balance could be investigated in ocean biogeochemistry models. In macronutrient manipulation studies, the putative effects of iron fertilization on the physical-chemical efficiency $e_{\text{phys-chem}}$ are simulated by assuming that iron fertilization reduces surface nutrient concentrations by formation and export of organic matter, which also removes a corresponding amount of dissolved inorganic carbon with standard stoichiometric ratios. Because of the absence of ecosystem and iron cycle model components, macronutrient manipulation studies are unable to simulate the biogeochemical response function, $R^{\text{C:Fe}}_{\text{iron utilization}}$. The patch Equatorial Pacific macronutrient depletion simulation of Gnanadesikan et al. (2003) using a Martin et al. (1987) power law remineralization profile gave an extremely low $e_{\text{phys-chem}}$ of 2.0% for the 100 yr response of a one-time, one-month nutrient depletion scenario. Identical simulations for 50 yr at the northwest Pacific SEEDS site by Matsumoto (2006) gave $e_{\text{phys-chem}}$~7% after 100 yr. The difference between these two sites is likely due to the mechanisms discussed by Jin et al. (2008) in their examination of $e_{\text{phys-chem}}$, namely the effective depth from which the DIC is removed by the nutrient depletion, and the thickness of the mixed layer, with shallower DIC removal depths and thinner mixed layers at the time of fertilization giving a higher efficiency of CO_2 removal from the atmosphere. The depth of the remineralization is also an important factor in the response: if all the excess organic carbon exported from the surface of the ocean is allowed to sink to the ocean floor before being remineralized, the efficiency rises to ~10% in the Equatorial Pacific and ~12% in the northwest Pacific.

By contrast with the macronutrient depletion scenarios, Gnanadesikan et al. (2003) obtained an efficiency of 42% at their Equatorial Pacific site when macronutrients were

BGD
6, 10381–10446, 2009

added. In their discussion of their two sets of simulations, Gnanadesikan et al. (2003) suggest that the macronutrient depletion scenario is essentially simulating the effect of an iron fertilization where the iron is added and then lost at the end of the nutrient depletion event, whereas the macronutrient addition scenario is effectively an iron added and permanently retained scenario. Biogeochemical models including the iron cycle will likely fall somewhere between the two extremes of $e_{\text{phys-chem}}$=2% and 42%, as is the case with the scenarios discussed in this paper as well as the simulation study of Aumont and Bopp (2006), who obtained an $e_{\text{phys-chem}}$ of 33% in their 100 yr simulation of iron stress relief (cf. also the $e_{\text{phys-chem}}$ of 10–25% obtained by Zeebe and Archer (2005), albeit with a different simulation approach).

How are we to move forward in this "sea of uncertainty" (cf. Buesseler et al., 2008) where both field experiments and model simulations disagree with each other by one or more orders of magnitude in critical parameters such as the physical-chemical efficiency and biogeochemical response function, and with only minimal understanding of why this is so? Clearly, a broad spectrum of experimental as well as modeling studies is required. As regards the models, ocean biogeochemical models with an explicit iron cycle as well as an ecosystem component, and which can therefore be used to examine both the biogeochemical response function $R^{\text{C:Fe}}_{\text{iron utilization}}$ and the physical-chemical efficiency $e_{\text{phys-chem}}$, have been in existence for several years now (e.g., Moore et al., 2002b; Aumont et al., 2003; Dutkiewicz et al., 2005; Tagliabue and Arrigo, 2006). These models have been used to examine the effect of iron on biological productivity and the ocean nutrient distribution (e.g., Moore et al., 2002a; Aumont and Bopp, 2006; Tagliabue et al., 2008; Schneider et al., 2008; Moore and Doney, 2007), as well as on the atmosphere in response to changes in dust delivery at present and during the ice ages (e.g., Bopp et al., 2003). A major motivation for the study described in this paper is one such sensitivity study carried out in an adjoint model by Dutkiewicz et al. (2006). The adjoint model makes it possible to efficiently calculate the separate effect of iron fertilization on a grid point by grid point basis for every single surface grid point in the model. A surprising finding from the Dutkiewicz et al. (2006) study was that the highest

BGD
6, 10381–10446, 2009

uptake of atmospheric CO_2 occurred when iron was added in the equatorial Pacific HNLC region, with a much smaller uptake resulting from iron addition in the Southern Ocean HNLC region. This result differs dramatically from what we would have inferred from earlier macronutrient manipulation studies such as those of KVHISOUTH shown in Table 1.

This disagreement between the Dutkiewicz et al. (2006) results and previous studies was the original stimulation for the organization of an Iron Fertilization Model Intercomparison Project (IFMIP) with the main initial purpose to examine the sensitivity of the iron fertilization response to the basic structure of the biogeochemistry models. The overall results of IFMIP will be described in a manuscript that is in preparation by Maltrud et al. In related work, Jin et al. (2008) carried out a series of sensitivity studies examining how the physical-chemical efficiency $e_{\text{phys-chem}}$ is related to the mixed layer thickness and depth within the surface ocean at which the enhanced removal of nutrients and DIC occurs. As part of this study, we undertook to examine the following questions:

1. What processes determine the physical-chemical efficiency $e_{\text{phys-chem}}$?
    a. Following on Jin et al. (2008), we show that the depth within the surface ocean at which the enhanced removal of nutrients and DIC occurs has a significant impact on the differential response between different fertilization sites.
    b. Following on Gnanadesikan et al. (2003), we show how the inclusion of a realistic atmospheric reservoir, which allows for the atmospheric CO_2 to drop in response to the iron fertilization thus leading to CO_2 escape from the global ocean, affects the overall physical-chemical efficiency. The IFMIP simulations all have a fixed atmospheric CO_2 concentration and thus overestimate the iron fertilization efficiency.
2. What processes determine the biogeochemical response function $R^{\text{C:Fe}}_{\text{iron utilization}}$?
    a. We examine how the ambient pre-fertilization environment of surface nutrient

BGD
6, 10381–10446, 2009

concentrations, light supply, and seasonal changes is linked to the biogeochemical response function. As expected, sites with higher initial surface nutrient concentrations have bigger responses unless low light and deep mixed layers interfere.

b. We probe how the ecosystem model affects the response by changing the frequency of iron addition, by relieving iron stress and seeing how the system responds, by comparing the effect of iron addition in one location vs. the others, and by comparison of some of our model characteristics with those of other groups that have done similar simulations.

c. Following on Gnanadesikan et al. (2003), we demonstrate that the retention time of added iron in the ocean has a major impact on the biogeochemical response function.

d. We show that the response of the nitrate cycles of fixation and denitrification to iron fertilization can have a major impact on the biogeochemical response function. In particular, the Equatorial Pacific HNLC region has a very low biological response function in our model due to a major loss of nitrate from the ocean by increased anoxia leading to increased denitrification.

Overall, we find in our model simulations that the efficiency of iron addition is indeed greatest in the Southern Ocean HNLC region and much smaller in the North and Equatorial Pacific HNLC regions, but that this has a lot to do with differences in how the ecosystem model component is constructed.

2 Model description

2.1 Physical and biogeochemical model

Details of the physical models used for this study are described in Appendix B. For ecology and biogeochemistry, we use an early generation of the GFDL TOPAZ model devel-

oped by Dunne et al. (see Supplementary Material http://www.biogeosciences-discuss.net/6/10381/2009/bgd-6-10381-2009-supplement.pdf). The model has eight dissolved inorganic variables: nitrate, ammonium, phosphate, silicate, oxygen, iron, carbon, and alkalinity. Biological processes are simulated with 5 functional groups, three that are solved explicitly (small and large phytoplankton as well as diazotrophs) and two that are solved implicitly (diatoms as a function of large phytoplankton, and coccolithophorids as a function of small phytoplankton). Grazing is modeled implicitly as described by Dunne et al. (2005), as is particulate organic matter. Small and large phytoplankton are assumed to have an N:P of 16:1 while diazotrophs have an N:P of 50:1 after Letelier and Karl (1998). Dissolved organic matter is modeled explicitly as consisting of a labile component with an N:P ratio of 16:1 and a lifetime of 3 months; and a semi-labile component with separate N and P components with lifetimes of 18 yr and 4 yr, respectively (cf. Abell et al., 2000). The model includes denitrification in both the water column when oxygen falls below 5 mmol m^{-3}, and in the sediments using the flux-based algorithm of Middelburg et al. (1996).

Phytoplankton growth rate is equal to a temperature-dependent maximum growth rate, times a dimensionless nutrient limitation term with a value between 0 and 1, times an iron-light co-limitation term also with a value between 0 and 1. The nutrient limitation term is the minimum of nitrogen dependence, modeled as in Frost and Franzen (1992) as modified by Sharada et al. (2005), or phosphorus or silicic acid dependence (for diatoms only), both modeled as Michaelis-Menten kinetics. Figure 1a–c shows the geographic distribution of which nutrient is limiting for each type of phytoplankton. The general pattern is one of nitrate limitation in the subtropics for both small and large phytoplankton, and phosphate limitation in the subtropics for diazotrophs. The Equatorial Pacific upwelling HNLC region and subpolar and polar HNLC regions of the North Pacific and Southern Ocean are generally replete (defined as $\geq$0.965) in P and N but limiting in Si for large phytoplankton (diatoms).

Iron and light limitation are simulated using a novel quota-based light-Fe colimitation approach developed by Dunne et al. (see Supplementary Material http://www.

BGD
6, 10381–10446, 2009

biogeosciences-discuss.net/6/10381/2009/bgd-6-10381-2009-supplement.pdf) based on fitting the observations of Sunda and Huntsman (1997). This approach allows "luxury uptake" of iron so that the plankton are very effective at taking up iron even when it does not result in an immediate increase in growth rate. The calculation of the growth rate is based on Geider et al. (1997) with the Fe:N ratio and light supply modulating the Chl:N ratio. The half saturation constant for iron uptake by small phytoplankton and diazotrophs is 0.1 μmol m^{-3}, and that for large phytoplankton is 0.3 μmol m^{-3}. The final value of the light-Fe colimitation term is shown in Fig. 1d–f. It is generally between 0 and 0.2 in the traditional HNLC regions for the large phytoplankton, and very near 1 everywhere else except the North Atlantic, where wintertime darkness reduces it to the 0.6 range. Small phytoplankton have the same pattern, but with less limitation. Diazotrophs are light and iron co-limited almost everywhere except where iron supply by dust is high.

The cellular C:Fe mole ratio that results from the independent Fe and N cycles varies between 56 000 and 300 000 for large phytoplankton and 4000 to 30 000 for diazotrophs, with a global mean C:Fe ratio in exported organic matter of 148 500 mol C:mol Fe. These cellular ratios are well within the bounds of the observations discussed in Sect. 1 and references therein.

Iron is removed from the ocean not only by phytoplankton uptake, but also by second order adsorption onto any particle form including ballast and particulate organic matter. It is remineralized along with organic matter in the water column and sediments. The removal of iron by adsorption at the surface of the ocean has a time scale of 10 yr or longer everywhere, which means that phytoplankton uptake is the dominant loss mechanism. By contrast, adsorption is the main mechanism for removal of iron in the deep ocean, where the removal time scale ranges between 40 and 300 yr at a depth of 2000 m. The aeolian flux of iron is that of Ginoux et al. (2001), with 2% of the iron assumed to be soluble in seawater. The total annual iron input from the atmosphere is 3.31×10^9 mol yr^{-1} with a sediment input of 0.68×10^9 mol yr^{-1}. The iron inventory in the model ocean after a 1000-yr spin-up is 575×10^9 mol, giving a mean residence time

BGD
6, 10381–10446, 2009

of 144 yr with respect to the combined dust and sediment inputs. This is within the bounds of previous estimates such as those discussed by Johnson et al. (1997). Since iron added by fertilization is treated the same as the "natural" iron, this means that the iron added by iron fertilization will remain in the ocean for decades to centuries before being scavenged.

Figure 2a–c shows a comparison of observed and model predicted annual mean phosphate at the surface of the ocean after a 1000-yr spin-up prior to carrying out the iron fertilization simulations. The correlation and relative standard deviation of surface phosphate in the model compared with the observations are 0.87 and 0.70, respectively; the root mean square error is 0.46 mmol m^{-3} of phosphate. For phosphate in the ocean as a whole, the correlation is 0.86 and the relative standard deviation is 0.87, which is comparable to the three models discussed by Schneider et al. (2008); and the root mean square error is 0.34 mmol m^{-3}. The model generally captures the spatial distribution of the high nutrient regions in the North and Equatorial Pacific and Southern Ocean, although it has too high phosphate in the tropics and subtropics and too low phosphate in the high latitudes compared with the observations. The amount of carbon sequestered from iron fertilization is closely tied to the change in unutilized or preformed nutrients (Gnanadesikan and Marinov, 2008; Marinov et al., 2008). We thus expect that our model would over-predict the response to iron fertilization in the tropics, and under-predict the response to fertilization in the high latitudes relative to a model that was forced towards the observed nutrients. In fact, that is exactly what we see in the regional scenarios of iron stress relief summarized in column 3 of Table 1 as compared with the nutrient depletion scenarios in the KVHISOUTH model, which in its control scenario is forced towards observed surface nutrients. The tropical response in our model is more than twice as large than in KVHISOUTH, and the Southern Ocean response is somewhat smaller, so that the Southern Ocean response is now only 3.7 times the tropical response rather than 8.5 times as in the nutrient depletion simulation.

Figure 2d–f compares the observed and modeled oxygen distribution at 300 m. We show this here because of the importance of denitrification for the response of the

BGD
6, 10381–10446, 2009

Equatorial Pacific to iron fertilization that we shall discuss later. The correlation and relative standard deviation of the model compared with the observations at this depth level are 0.89 and 1.10, respectively, with a root mean square error of 43.3 mmol m^{-3}. For the ocean as a whole, the correlation and relative standard deviation are 0.88 and 1.18, respectively, with a root mean square error of 56.0 mmol m^{-3}. In general, the model over-predicts the oxygen at 300 m, which might lead one to expect lower denitrification. However, the volume of water in the model with oxygen concentrations less than 10 mmol m^{-3} is in fact almost 7 times as great as the corresponding volume in the observations (27.2×10^{15} m^3 vs. 4.0×10^{15} m^3, respectively). This problem of too much suboxia is common to all the biogeochemical models we are familiar with, though we would also note that the data are also problematic at such low oxygen levels.

2.2 Iron fertilization simulations

The iron fertilization simulations are carried out at the end of a 1000-yr spin-up of the biogeochemistry model at which time the air-sea CO_2 flux is drifting at a rate of 0.08 Pg C yr^{-1}. The iron fertilization scenarios are based on the IFMIP protocol as will be described in a manuscript that is in preparation by Maltrud et al., which, in turn, is based to the greatest extent possible on the MIT adjoint model study of Dutkiewicz et al. (2006). The adjoint model makes it possible to efficiently calculate the separate effect of iron fertilization on a grid point by grid point basis for every single surface grid point in the model. However, this option was not available to other IFMIP participants and so we chose to do patch fertilization at the four representative locations given in Table 2 and illustrated in Fig. 2. These sites are all in the Pacific Ocean and span the three major HNLC regions of the North, Equatorial, and South Pacific. Motivated by the Southern Ocean biogeochemical divide described by Marinov et al. (2006), to the north of which nutrient depletion affects primarily the global biological export production, and to the south of which nutrient depletion affects primarily the air-sea balance of carbon dioxide, we chose two sites in the Southern Pacific: the subpolar region of the Southern Ocean north of the divide, and the polar Ross Sea region south of the divide.

BGD
6, 10381–10446, 2009

The size of the iron patches for each IFMIP model was supposed to be as close as possible to the size of the cell area of the MIT grid location closest to the patch. However, in our model simulations, we chose to fertilize an integral number of grid cells that would make the area of each of our four fertilization sites as close as possible to each other so that the total amount of iron added in each case would be approximately the same (see columns 3 and 4 of Table 2). Following Dutkiewicz et al. (2006), bioavailable iron is added to the ocean continuously at a rate of 0.02 mmol m^{-2} yr^{-1}, which was chosen by them as representative of the background aeolian flux in their model, which ranges from a low of 0.001 to 0.5 mmol m^{-2} yr^{-1}. The original IFMIP specification was that simulations were to be carried out for 10 yr, but we show here results of simulations that have been carried out for 100 yr.

We performed additional sensitivity studies using the same IFMIP bioavailable iron input of 0.02 mmol m^{-2} yr^{-1}. The principal ones we use in our discussion below are: 1) a one month one time fertilization, which is the time scale used by Gnanadesikan et al. (2003); 2) fertilization for one month per year for 10 yr (10× as much iron as case 1); 3) fertilization for one month per year for 100 yr (100× as much iron as case 1); and 4) continuous fertilization for 100 yr as in Dutkiewicz et al. (2006) (1200× as much iron as case 1). In what follows, we shall refer to these four scenarios as the 1×, 10×, 100×, and 1200× cases, respectively. In the one month and one month per year simulations, the month of iron addition was chosen to be immediately after the spring bloom when the iron concentration drops below the 0.01 μmol m^{-3} contour (see Fig. 3i–l and column 5 of Table 2). With four different fertilization locations, this represents a total of 4×4=16 separate simulations.

2.3 Control simulations

A control simulation with no iron fertilization is carried out simultaneously with the iron fertilization scenarios. Figure 3 shows several key diagnostics from the control simulation at each of the four fertilization sites. All the figures are depth vs. time contour plots for a period of two years. Each also includes the KPP mixed layer depth (see Ap-

BGD
6, 10381–10446, 2009

pendix B for definition). Consider first the combined seasonality of the KPP mixed layer depth and irradiance shown in Fig. 3a–d. At PAPA, the Equatorial Pacific site, and the subpolar Southern Ocean site, the KPP mixed layer depth varies seasonally but never goes deeper than 100 m. By contrast, the Ross Sea site has a KPP mixed layer depth of greater than 100 m for 6 months of the year. As with mixed layer depth, the light supply at the Equatorial Pacific site has very little seasonal variability. However, the light seasonality gets progressively stronger as one goes from PAPA to the Southern Ocean site and Ross Sea site, where irradiance is below 5 W m^{-2} for 6 months a year. One would expect that adding iron to the ocean during the wintertime periods of deeper mixed layers and low light levels at the PAPA, the South Pacific site, and, especially, the Ross Sea site, would be less efficient than at other times of the year. Indeed, this seasonality of the light supply and mixed layer depths is, we believe, one reason that Dutkiewicz et al. (2006) found a less efficient response to continuous iron addition in the high latitude Southern Ocean than in the Equatorial Pacific.

In Fig. 3e–p, we show the time evolution of nitrate, iron, and chlorophyll at the four sites in the control simulation. We see from the nitrate and chlorophyll contour plots that all four locations fit the classical definition of an HNLC regime, with nitrate concentrations that never become depleted, and chlorophyll concentrations that drop precipitously after the spring bloom at a time when the nitrate concentrations, light supply, and mixed layer depth are all still ideal for phytoplankton growth. We note that PAPA and the Equatorial Pacific site drop to relatively low nitrate concentrations during the summertime nutrient minimum: 4.3 mmol m^{-3} and 3.7 mmol m^{-3}, respectively; as contrasted with the much higher summertime nutrient minima of 17.1 and 12.5 mmol m^{-3} at the South Pacific site and Ross Sea sites, respectively. All else being equal, we might expect a greater conversion of preformed to remineralized nutrients and thus a bigger response of the air-sea CO_2 balance to fertilization at the latter two sites (cf. Marinov et al., 2008; Gnanadesikan and Marinov, 2008).

BGD
6, 10381–10446, 2009

3 Results

We discuss first the perturbation export production, then the nitrate, iron, and oxygen redistribution resulting from iron fertilization, and finally the perturbation air-sea CO_2 flux.

3.1 Response of export production

The initial response of the annual particulate carbon export (POC plus $CaCO_3$) to iron fertilization is very rapid in this model (Fig. 4a–d), with the peak export in the 1 month per year fertilization scenarios (1×, 10×, and 100×) occurring during the month of fertilization, then dropping back to near zero after 2 to 3 months. Except at the Equatorial Pacific site, the annual carbon export production continues to grow modestly from one year to the next as more iron is added in the 10×, 100×, and 1200× cases until it saturates on a time scale of a few decades in the 100× and 1200× cases (Fig. 4f–h). When fertilization is terminated in the 1× and 10× cases, the perturbation export production plunges almost instantaneously back to near zero. The behavior at the Equatorial Pacific site is atypical because of a major loss of nitrate by denitrification, as discussed in Sect. 3.2.

As one would expect from the relatively constant annual export production during the fertilization period in Fig. 4f–h, the cumulative total carbon export results in Fig. 4j–l show an almost linear increase with fertilization time at all sites (again with the exception of the Equatorial Pacific). Furthermore, the linear scaling with amount of iron added works reasonably well even after the fertilization is terminated, with the 1× and 10× cases showing roughly 1/100 and 1/10 of the cumulative export production in the 100× case, and the 1200× case showing approximately 12 times the response of the 100× case. (Note that the vertical axes of Fig. 4i–l are scaled according to the total amount of iron added.) Aside from the Equatorial Pacific, the one significant exception to this scaling is the huge drop in the cumulative Ross Sea response to iron fertilization in the 1200× case vs. the 100× case. This drop is due to the highly unfavorable

BGD
6, 10381–10446, 2009

wintertime mixed layer and irradiation conditions (see Fig. 3d) which results in Ross Sea biological production shutting down completely for 5 months from June to October (Fig. 3p). Iron added during this period in the 1200× case is swept out of the surface into the deep ocean without influencing the export production (see Sect. 3.2).

A more detailed analysis of the biological response to the iron fertilization simulations and a comparison with observations is given in Appendix C.

3.2 Response of iron, nitrate, and oxygen distributions

We show in Fig. 5 an analysis at year 100 of the impact of the 1200× iron fertilization simulation on the horizontally integrated vertical iron, nitrate, and oxygen distributions, and in Fig. 6, the impact of the 1200× simulation on the vertically integrated horizontal distributions of nitrate and oxygen. As might be expected, Fig. 5 shows that the addition of iron increases the iron inventory at all locations, that the enhanced removal of nutrients from the surface ocean causes a downward displacement of the perturbation nitrate distribution (reduced in the upper ocean and increased at depth), and that there is an overall reduction in the oxygen inventory (except right near the surface due to photosynthetic production of oxygen at the Equatorial Pacific site).

Comparison of Figs. 5 and 6 shows that the nitrate surplus is largely a deep ocean phenomenon confined to the vicinity of the four sites, whereas the nitrate deficit is largely an upper ocean phenomenon with a widespread distribution. As a consequence of the widespread upper ocean nitrate reduction, the cumulative perturbation export production away from the fertilization sites is generally reduced in the subtropical gyre regions, which are already nitrate-limited in the control scenario (Fig. 6i–l), but have adequate light and iron (Fig. 1) such that the additional iron has no impact (cf. Gnanadesikan et al., 2003).

At year 100, the oxygen deficit in the fertilization scenarios is still largely confined to the vicinity of the four sites, which means the north Pacific for PAPA, the eastern tropical Pacific for the equatorial Pacific site, and the circumpolar region for the Southern Ocean and Ross Sea sites, though with some influence on northward flowing bottom waters

BGD
6, 10381–10446, 2009

in the Ross Sea case. In the particular case of the Equatorial Pacific, the reduction in oxygen is concentrated in the vast region of suboxia (defined as O_2<5 mmol m^{-3}) of the eastern tropical Pacific shown in Fig. 2e. Reduced oxygen due to fertilization at this site thus causes an expansion of the suboxic zone and an increase in the loss of nitrate by denitrification (which in this model is turned on when oxygen is <5 mmol m^{-3}). The cumulative 100 yr nitrogen budget given in Table 3 shows that denitrification resulting from iron fertilization at the Equatorial Pacific site totals almost 5 Tg of N over 100 yr. The large cumulative N_2 fixation of ~1 Tg N resulting from iron fertilization at this site is too small to counterbalance the denitrification, and the cumulative loss of nitrate comes to almost 4 Tg N over the 100 yr period. This overall response of enhanced denitrification exceeding enhancement of nitrogen fixation is unexpected. It goes in the opposite direction from the feedback found by Moore and Doney (2007) in their model study, which showed an increase in the marine fixed nitrogen inventory, albeit with global iron stress relief. The influence of iron fertilization on the nitrate inventory at the other three sites is more modest. All three show a slight increase of oxygen in the eastern tropical Pacific, and a corresponding decrease in water column denitrification. All three also show an increase of surface N_2 fixation. Overall, PAPA and the Southern Ocean show a small increase in the nitrate inventory, while the Ross Sea is almost neutral due to an increase in sediment denitrification.

3.3 Response of air-sea CO_2 flux

One of the findings emphasized by Gnanadesikan et al. (2003) was the large scale degassing flux that occurs throughout the world ocean after iron fertilization. This degassing flux is due to the reversal in the atmospheric CO_2 gradient that occurs as CO_2 is removed from the atmosphere by iron fertilization. The back flux of CO_2 from the ocean to the atmosphere is a phenomenon that applies to any reduction of anthropogenic CO_2 sources or enhancement of sinks, and has not always been taken into consideration when comparing various carbon mitigation options with each other (though it should be). In this section, we follow the IFMIP protocols in showing only sim-

BGD
6, 10381–10446, 2009

ulations with a fixed atmospheric CO_2 at a pre-industrial partial pressure of 278 μatm. In Sect. 4, we describe sensitivity studies that show how the results change when the atmospheric reservoir of CO_2 is allowed to drop as iron fertilization removes CO_2.

A comparison of the air-sea fluxes from the 1× simulations in Fig. 7a with the export production in Fig. 4a shows that the peak in the air-sea flux occurs about a month after the peak in the export production. The CO_2 uptake pulse extends over about 3 months at the Ross Sea site, 9 months at the PAPA and Southern Ocean sites, and 15 months at the Equatorial Pacific site. The Equatorial Pacific site best reflects the time scale of air-sea equilibration in a somewhat more stable situation where the DIC deficit generated by the iron fertilization lasts year around (Fig. 8j), whereas the other sites, particularly that in the Ross Sea, are more strongly influenced by seasonality, with the deficit deficit generated by the export pulse becoming extremely small in the wintertime (Fig. 8i, k, l). In particular, as Fig. 8l shows, the surface DIC concentration at the Ross Sea site is restored to its control wintertime value for 5 months of the year and only departs from it significantly for 3 to 4 months of the year.

A major feature of the annual perturbation atmospheric CO_2 uptake shown in Fig. 7e–h is that the CO_2 uptake by the ocean plummets into the negative range as soon as iron fertilization ends in the 1× and 10× scenarios, and that, unlike the export production, it drops lower and lower over time as the fertilization is continued over 100 yr in the 100× and 1200× cases. The only exception to this drop is at the Ross Sea site in the 1200× case, where the annual air-sea CO_2 flux remains nearly constant over time. The rebound effect of CO_2 escaping back to the atmosphere upon cessation of fertilization that we find in the 1× and 10× cases has been demonstrated in many of the nutrient depletion scenarios (e.g., Sarmiento and Orr, 1991), and was also found in the ecosystem/model simulation of Aumont and Bopp (2006). However, cessation of fertilization in nutrient depletion scenarios occurs by immediately allowing restoration of surface nutrients back to their normal control values, and is thus likely to exaggerate the return flux of sequestered CO_2; and the model of Aumont and Bopp (2006) has an interactive atmosphere and would therefore have a significant contribution to the

BGD
6, 10381–10446, 2009

return flux due to lowered CO_2 in the atmosphere. Here we find that the rebound effect occurs even with fixed atmospheric CO_2 in our 1× and 10× simulations (Fig. 7e, f). Furthermore, even the continued addition of iron in the 100× and 1200× cases is not able to prevent the annual uptake of CO_2 from the atmosphere from dropping over time (Fig. 7g, h) despite the fact that the magnitude of the export production remains high (except at the Equatorial Pacific site; Fig. 4g, h). This drop off has a major negative impact on the efficiency of iron fertilization, as we shall see in Sect. 4.1.

Another interesting result in the 1×, 10×, and 100× atmospheric CO_2 uptake scenarios is that the cumulative Ross Sea site uptake is much greater than the Southern Ocean uptake (Fig. 7i–k and Table 4a) despite the perturbation export production of these two being virtually identical in the 10× and 100× simulations and very similar in the 1× case (Fig. 4i–k). We believe that the enhanced uptake at the Ross Sea site is due mostly to the shallowness of the summertime mixed layer and of the DIC removal per Jin et al. (2008), as discussed below. The relative behavior of the Ross Sea and Southern Ocean sites reverses in the 1200× scenario due to the previously discussed wintertime shut down at the Ross Sea site.

4 Discussion

We begin with a discussion of the efficiency of iron fertilization (the cumulative atmospheric CO_2 uptake divided by the cumulative iron addition as in Eq. 1) and the processes that determine it, followed by a discussion of the sensitivity studies that we carried out.

4.1 Efficiency of fertilization

Figure 9 shows the fertilization efficiency that we defined in Eq. (1). Except at the Equatorial Pacific site, where denitrification distorts the results, the biogeochemical response function has a value of between ~100 000 and ~250 000 mol C:mol Fe (Fig. 9g–

BGD
6, 10381–10446, 2009

i). This spans the global mean C:Fe mole ratio of the export production in the control simulation of 148 500, and is comparable to the observed intracellular C:Fe ratios discussed in the Introduction. The observations that are most comparable to the simulations we performed are the seasonal integrals at Kerguelen and Crozet. Our biogeochemical response function lies between the export ratios observed at Kerguelen, and those detected at Crozet. Again except for the Equatorial Pacific, our physical chemical efficiencies start out near 1 in some cases, but then drop down to the range of 35% to 65% in the 100× case, which is in excellent agreement with the Kerguelen and Crozet estimates of 37% and 69%, respectively (Fig. 9d–f). Appendix C has a more detailed comparison of the model with observations.

From Fig. 9a–c and Table 4b, we see that by far the most efficient fertilization site is the Ross Sea, except in the 1200× case, where the Southern Ocean site becomes dominant. The Ross Sea in particular has a very high CO_2 uptake to iron fertilization mole ratio of 150 000 to 188 000 for the 1×, 10×, and 100× simulations for the entire period of the fertilization. However, the Ross Sea efficiency plunges well below the other sites for the first ∼50 yr of the 1200× continuous fertilization scenario due to the ineffectiveness of iron fertilization during the polar winter. Next in efficiency is the Southern Ocean, which is about half as efficient as the Ross Sea in the 100× case and less than that in the 1× and 10× cases, but exceeds the Ross Sea in the 1200× case. Both PAPA and the Equatorial Pacific site are by far the least efficient, with C:Fe ratios that are about half of the Southern Ocean site for the 10×, 100×, and 1200× scenarios. Because the efficiency in the 1× scenario for all four sites is extremely noisy due to the small size of the iron fertilization perturbation relative to the background variability in this scenario, it has not been included in Fig. 9.

What accounts for the differences in responses to the iron addition between the four regions illustrated in Fig. 9a–c? To answer this question, we find it useful to analyze the results in terms of the physical-chemical response function $e_{\text{phys-chem}}$ and the biogeochemical response function $R^{\text{C:Fe}}_{\text{iron addition}}$. Figure 9d–i shows the results of this analysis for the 10×, 100×, and 1200× simulations. The first result we draw attention to is that

BGD
6, 10381–10446, 2009

the biogeochemical response function in Fig. 9g–i is quite different at the Equatorial Pacific site than at any of the others. The Equatorial Pacific site has less nitrate in the control scenario to start with (see Fig. 8f), and in addition, as discussed in Sect. 3.2, there is loss of nitrate by denitrification due to an increase in the volume of suboxic waters. The nitrate loss due to fertilization at the Equatorial Pacific site already begins to lower the biological export production within one to two decades after the initiation of fertilization (see Fig. 4), and is the principal reason that the Equatorial Pacific site has such a low efficiency in the 10×, and 100× cases shown in Fig. 9a, b. The only reason that the Equatorial Pacific site has a higher efficiency than PAPA and the Ross Sea in the continuous fertilization 1200× case of Fig. 9c (until the Ross Sea site catches up at almost 70 yr) is because of the reduced effectiveness of the iron addition at PAPA and the Ross Sea during the wintertime.

The anomalous decrease of the perturbation carbon export $\Delta\Phi_{export}^{Org\,C\&CaCO_3}$ at the Equatorial Pacific site that is documented in Fig. 4i–l lowers the biogeochemical response function shown in Fig. 9g–i, and causes the physical-chemical response function shown in Fig. 9d–f, to sweep upwards after first decreasing like the other fertilization sites. This behavior is due to an unusual biological response, namely denitrification, and not to the biological, physical, and chemical processes we are trying to diagnose with the physical-chemical response function. We thus will not comment any further on the Equatorial Pacific site results in Fig. 9.

Turning to the other three sites, we see first that the Ross Sea and Southern Ocean are similar to each other in terms of the biogeochemical response function (Fig. 9g, h), except when the fertilization is extended to include the Austral winter in the 1200× case (Fig. 9i). In this latter case the deep wintertime mixing in the Ross Sea (Fig. 3) causes it to plummet to the bottom of the stack. Where the Ross Sea clearly stands out above the others is in its high physical-chemical response function (Fig. 9d–f, excluding the anomalous Pacific site). Jin et al. (2008) show in their model simulations that the physical-chemical response function depends primarily on the depth at which the enhanced formation of organic matter is occurring in response to iron addition. We show

BGD
6, 10381–10446, 2009

in Fig. 10 that the index they use to calculate the depth of the enhanced production does indeed show a strong shallow bias of the Ross Sea relative to the other locations. With such a shallow removal of carbon from the water column, a higher percentage of the CO_2 that is taken up by the biota with iron addition comes from the atmosphere as compared to other sites. A necessary condition for this shallow response to the iron addition is that nutrients should be high at the surface, which Fig. 8 shows that they are even at the time of the nutrient minimum. However, the same can be said of the Southern Ocean site. Another necessary condition for a shallow response is that the mixed layer should be shallower, which is indeed the case during the period of fertilization at the Ross Sea site, but not the Southern Ocean site (see Fig. 3).

By contrast with the Ross Sea, the Southern Ocean and PAPA sites have similar physical-chemical response functions (Fig. 9d–f). The reason that the Southern Ocean has much higher iron fertilization efficiency than PAPA is because of the biogeochemical response function, which is far greater at the Southern Ocean site than at PAPA (Fig. 9g–i) due to the higher initial nutrient concentrations at this location (Fig. 8).

4.2 Model sensitivity studies

Three sets of model sensitivity studies were carried out as part of our study:

(1) Coupling to an atmospheric reservoir: The IFMIP protocol specified a fixed atmospheric CO_2 concentration following the design of the original study by Dutkiewicz et al. (2006). However, we expect that as CO_2 is removed from the atmosphere by iron fertilization, this will lead to a reversal in the global air-sea CO_2 gradient relative to what it would have been without the CO_2 removal. Much of the CO_2 taken up locally in the iron fertilization region will thus escape back to the atmosphere in the rest of the ocean, as demonstrated by Gnanadesikan et al. (2003) (cf. also Oschlies, 2009). In order to examine the magnitude of this feedback, we carried out a set of sensitivity studies in which the IFMIP simulations were repeated but in an ocean model that was coupled to an atmospheric reservoir. The CO_2 in the atmospheric reservoir was fixed at 278 ppm

BGD
6, 10381–10446, 2009

in the model spin-up, and then allowed to vary in both the control and iron fertilization simulations for the period of the iron fertilization. We leave for future simulations the inclusion of secondary effects that will also impact the iron fertilization efficiency, including a more realistic atmospheric CO_2 trajectory driven by fossil fuel CO_2 emissions and terrestrial sources and sinks (cf. Joos et al., 1991; Oschlies, 2009) as well as the impact of climate on the terrestrial and oceanic sources and sinks.

Figure 11a and Table 5 show that including a variable atmosphere allows 20% of the CO_2 taken up in the fixed atmosphere 1200× simulation to escape after only 10 yr, and ~50% after 100 yr. The 100× fertilization is very similar, but for the shorter-term 1× and 10× cases, the reduction of CO_2 uptake is more drastic, getting as high as 76% after 100 yr in the PAPA 1× case. This is clearly a major effect that cannot be ignored in model simulations. Note from Fig. 11b that the biogeochemical response function is identical to that of the 1200× simulation with a fixed atmosphere, as would be expected.

(2) Amount of iron added: The per unit area iron flux of 0.02 mmol m^2 yr^{-1} in the standard 1200× simulation was chosen by Dutkiewicz et al. (2006) as representative of the background aeolian flux in their model, which ranges from a low of 0.001 to 0.5 mmol m^{-2} yr^{-1}. In none of the 1200× simulations was this flux large enough to deplete surface nutrients even at the time of the nutrient minimum (see Fig. 8). We carried out sensitivity studies with 5, 10, 100, and 1000 times as much iron flux as in the 1200× simulation in order to determine how far we could go towards depleting the nutrients before something else became limiting. As we see in Fig. 8, three of the four sites are nearly depleted by the time the iron flux is increased by 5 times the 1200× case, and the Southern Ocean becomes depleted with an iron flux that is somewhere between 10 and 100 times the 1200× case. Note, however, that, except at the Equatorial Pacific site, and to a lesser extent at the PAPA site, this depletion of nutrients can only be accomplished at the time of the nutrient minimum. Because of the seasonality of the light supply and mixed layer depth, the nutrient concentration at the time of the

BGD
6, 10381–10446, 2009

nutrient maximum at the other sites is almost unaffected by the iron flux.

(3) Iron retention: A 1200× simulation was carried out in which the added iron was assumed to be scavenged from the ocean permanently once it is taken up by biology. We refer to this as the "iron added and removed" simulation. Our intention was to examine the explanation of Gnanadesikan et al. (2003) for the ratio of ~1:20 in CO_2 uptake efficiency (2% vs. 42%) between the simulations that they characterized as behaving like an iron added and removed scenario, and those they characterized as behaving essentially like iron added and retained simulations. Since their model did not include an explicit parameterization of iron cycling, their equivalent to our definition of the iron fertilization efficiency given in Eq. (2) replaces the iron addition term in the denominator with the carbon export during the one month of fertilization, which we symbolize as $\Delta\Phi^{POC\,\&\,CaCO_3}_{export}$ (fertilization period), i.e.,

$$\frac{\Delta\Phi^{CO_2}_{air-sea}}{\Delta\Phi^{POC\,\&\,CaCO_3}_{export}\,(\text{fertilization period})}. \tag{3}$$

The carbon export during the fertilization period is taken to be representative of the initial iron addition.

Figure 11c, d shows the ratio of our 1200× iron added and lost scenario to our standard 1200× scenario for the physical-chemical response function and our biogeochemical efficiency. Figure 12 shows the efficiency of iron retention in the standard 1200× scenario. At the end of 100 yr, ~60% of the added iron is still in the ocean, whereas in the iron added and lost scenario, only the most recently added iron is present. Figure 11c shows that our iron added and lost simulations have almost the same physical-chemical response function as the standard 1200× simulations at all the sites. The EqPac site is a little high because the iron added and lost simulation does not have as much denitrification as the standard 1200× scenario. The biogeochemical efficiency ratios in Fig. 11d confirm that it is the continued ability of retained

BGD
6, 10381–10446, 2009

iron to maintain the flux of carbon out of the surface at a high level that is principally responsible for the much higher efficiency of the standard 1200× scenario over the iron added and removed scenario. Indeed, the EqPac site has 1/20 as much CO_2 removal from the atmosphere in the iron added and removed simulation than in the standard 1200× scenario, which is consistent with the difference that Gnanadesikan et al. (2003) saw in their simulations. Jin et al. (2008) suggest in their analysis that at least part of the difference in the two model simulations of Gnanadesikan et al. (2003) appears to be due to an inadvertent effect of the way they designed their models, in which the iron added and retained scenario is actually removing carbon from the entire euphotic zone, whereas the iron added and removed scenario is removing carbon only from the base of the euphotic zone, but our results support Gnanadesikan et al. (2003) in their suggestion that most of the effect is due to the assumptions that were made regarding the role of iron cycling (i.e., whether iron is added and removed vs. whether it is added and retained).

4.3 Alternate growth formulation

One of the limitations of this model's formulation of iron limitation of phytoplankton growth was the need to utilize elevated values of the maximum growth rate $P_{C_{max}}$ (see Supplementary Material http://www.biogeosciences-discuss.net/6/10381/2009/bgd-6-10381-2009-supplement.pdf) compared to observations of phytoplankton growth under ideal conditions. In order to examine how the results might change with a more realistic maximum growth rate, we carried out sensitivity studies using a Liebig formulation for the dependence of phytoplankton growth rate on the chlorophyll to carbon ratio (see Supplementary Material http://www.biogeosciences-discuss.net/6/10381/2009/bgd-6-10381-2009-supplement.pdf) and lower maximum zero-temperature-normalized growth rates of $0.98\,d^{-1}$ as observed in the SEEDS experiment for *Chaetoceros debilis* (Tsuda et al., 2003). This modification resulted in only a modest 1–2% change in the iron fertilization CO_2 uptake relative to the base formulation.

BGD
6, 10381–10446, 2009

5 Conclusions

We emphasize the following results from our study:

(1) As regards the atmospheric CO_2 uptake efficiency (cumulative CO_2 uptake divided by cumulative iron addition), our model shows a large response to iron addition at all four of our sites if iron is added for one month per year during the growing season. The atmospheric CO_2 uptake efficiency is by far highest at the Ross Sea site, with the Southern Ocean responding at about half the efficiency, and the PAPA and Equatorial Pacific trailing behind. Our results are thus consistent with the findings from the regional nutrient depletion simulations summarized in Table 1. Judging from our own continuous fertilization 1200× scenario, where the Ross Sea efficiency collapses, part of the reason Dutkiewicz et al. (2006) found maximum efficiency in the tropics and minimum efficiency in the Southern Ocean region is because they added iron year round including during the wintertime when the iron can get transported out of the surface without affecting biological export production. Another reason is because their phytoplankton maximum growth rate is more limited by light and less sensitive to iron, as will be explained below.

The Ross Sea stands out above all other locations as a place where once atmospheric CO_2 is sequestered, it tends to stay sequestered over at least a century time scale (Fig. 7e, f). It also has a high physical-chemical efficiency (Fig. 9d, e) due to the fact that the CO_2 is being removed very shallow in the euphotic zone (Fig. 10) and because of the shallower mixed layer. Because the Ross Sea site is well south of the biogeochemical divide defined by Marinov et al. (2006), it has a less deleterious effect on low latitude biological productivity than the Southern Ocean site. On the other hand, the local effects on biological production and the reduction in deep oxygen that then spreads as a tongue into the Pacific Ocean are major undesirable side effects (Figs. 5 and 6), and the issue of verification of the CO_2 uptake is at least as serious here as anywhere else.

BGD
6, 10381–10446, 2009

The Equatorial Pacific and PAPA sites are less efficient as sites for atmospheric CO_2 sequestration. The Equatorial Pacific site is highly unfavorable because of the huge negative impact that fertilization at this site may have on the nitrate inventory and thus on global biological productivity.

(2) We examined whether additional iron could lead to depletion of nutrients during at least part of the year. Figure 8 shows the annual mean nitrate concentration, and the concentration at the time of the summertime nutrient minimum for simulations in which the iron addition to the ocean was increased by 5, 10, 100, and 1000 times the 1200× flux. These results show that all the stations can be driven to zero nitrate in the summer time, but only the Equatorial Pacific can be driven to zero mean nitrate year around. In fact, in the Southern Ocean and Ross Sea, wintertime light limitation causes the nutrient concentration to recover all the way to its normal wintertime maximum even in the highest iron flux case, testifying to the effectiveness of the circulation in returning nutrients to the surface in these two regions.

The ability of our model to completely draw down nitrate during the summertime nutrient minimum in the Southern Ocean is in contradiction to the similar analyses of Mongin et al. (2007), and Aumont and Bopp (2006), in both of which cases the model became light limited. Dutkiewicz et al. (2006) also find greater light sensitivity than iron sensitivity in their model. The differences between all these models are complex and subtle. What we can say about our model is that it has a relatively high half-saturation constant for the dependence of large phytoplankton (which dominate iron fertilized blooms) on iron, $0.3\,\mu\mathrm{mol\,m^{-3}}$. This means that our model will in general be more sensitive to additional iron. Moreover, in our model the sensitivity to light is itself dependent on iron through the fact that additional iron allows for more chlorophyll synthesis, which greatly lowers the light sensitivity under iron replete conditions. For example, the half-saturation light level at the Southern Ocean site is only $\sim 3\,\mathrm{W\,m^{-2}}$ for iron-replete conditions as compared with the fixed value of $20\,\mathrm{W\,m^{-2}}$ used by Dutkiewicz et al. (2006) (though for iron concentrations of $0.1\,\mu\mathrm{mol\,m^{-3}}$ our half-saturation light level is closer to $12\,\mathrm{W\,m^{-2}}$). Thus, under iron fertilization our model is much less light limited than

other models. The treatment of iron-light colimitation in many models such as those of Mongin et al. (2007) gives increased limitation under conditions of increased growth rate. As discussed in Galbraith et al. (2009), this behavior is common in current model formulations, particularly ones where only the impacts of iron concentration on growth rates are modeled. In fact, observational studies such as those of Hiscock et al. (2008) show that quantum yield and chlorophyll to carbon ratio also increase under iron fertilization. As noted by Galbraith et al. (2009) only more detailed studies that parse out different phytoplankton physiological responses can properly constrain which models are most correct.

(3) The back flux of CO_2 from the ocean when a realistic atmospheric reservoir is included is substantial (Fig. 11a and Table 5; cf. Gnanadesikan et al., 2003). We strongly recommend that this effect should be taken into account when comparing various CO_2 sequestration scenarios with each other, particularly as it is sensitive to the time period of the sequestration. By the 100th year of the 1200× simulation, half of the CO_2 that is absorbed by the model with no atmospheric reservoir is lost back to the atmosphere in the model with a realistic atmospheric reservoir. In the case of the 1× simulation, the escape of sequestered carbon due to this effect is of order 70% and greater.

(4) When the iron added to the ocean follows the same behavior as the background "natural" iron cycle, as in our standard iron fertilization simulations, it is retained in the ocean for a long period of time (Fig. 12) and continues to play a role in increasing the biological productivity (as illustrated by the contrast with the simulation where iron was added then lost, Fig. 11d) and maintaining lower surface nutrient concentrations. By contrast, the physical-chemical efficiency is insensitive to whether the iron is retained or lost (Fig. 11c).

Additional findings which were already covered by the studies of Gnanadesikan et al. (2003) and Matsumoto (2006) include the difficulty of detecting the air-sea flux of CO_2 across the air-sea interface, a topic we have not investigated further here as we have nothing new to add; the negative impacts of the fertilization on downstream

BGD
6, 10381–10446, 2009

biological productivity, which we have discussed but not emphasized; and the extraordinarily low efficiency of iron fertilization in removing CO_2 from the atmosphere in an iron added and then lost scenario which is intended to mimic the comparable scenario in Gnanadesikan et al. (2003) and Matsumoto (2006). Our model behaves much more like the high efficiency scenarios of macronutrient addition, which Gnanadesikan et al. (2003) claimed was analogous to an iron added and retained scenario.

Based on our model simulations, we would suggest the following as important unknowns that will have a major impact on predictions of the CO_2 removal that results from iron fertilization:

(1) Processes that determine the physical-chemical efficiency:

The work of Jin et al. (2008) and our results here (Figs. 9a–c, and 10) suggest that the efficiency of CO_2 removal from the atmosphere is highly sensitive to the exact depth at which the biological uptake of CO_2 occurs as well as the thickness of the mixed layer. We need observational tests of this finding and we need to understand more about natural processes affecting the depth of this removal.

(2) Processes that determine the biogeochemical response function:

(a) The co-dependence of light and iron and how different formulations of this co-dependence affect the response of ecosystem models to changes in the iron supply. A model comparison study and associated experimental work would be very useful in helping to set up a standard set of simulations that would highlight critical responses of the models and test and improve them.

(b) The long-term fate of the added iron, which has a major impact on the biogeochemical response function (Fig. 11d). This represents an important uncertainty in current models of the iron cycle, which vary substantially in the rates of input and removal of bioavailable iron.

(c) What controls the size of the eastern tropical denitrification regions in models, which is too large in our model as well as in all of the other models we have

BGD
6, 10381–10446, 2009

examined, and which causes the tropics to be the worst location for iron fertilization in this study.

(d) How the air-sea balance of CO_2 is associated with changes in the inventory of remineralized nutrients in the ocean. We have had great success in analyzing this link for large-scale macronutrient depletion simulations (cf., Marinov et al., 2008; Gnanadesikan and Marinov, 2008), but this has not been done as yet for patch scale iron fertilization simulations.

Appendix A

Definition of variables

We define the flux of tracers such as Fe, organic matter, $CaCO_3$, or CO_2 across the air-sea interface or a given depth level, as f in mol m^2 yr^{-1}. We further define the area integral of this flux as

$$F = \iint f\,dx\,dy \tag{A1}$$

with units of mol yr^{-1}, and the cumulative area and time integral as

$$\Phi = \int_0^\tau F\,dt \tag{A2}$$

with units of mol. Finally, we define the perturbation of the flux f, the area integrated flux F, or the area and time integrated flux Φ as

$$\Delta(\ ) = (\ )_{\text{fertilization}} - (\ )_{\text{control}} \tag{A3}$$

Here, the subscript fertilization refers to the patch iron fertilization scenario and control refers to the control scenario with no patch iron fertilization.

BGD
6, 10381–10446, 2009

Appendix B

Physical model

The circulation model used in this study is based on the ocean component of the GFDL CM2.1 global coupled climate model (Griffies et al., 2005b; Gnanadesikan et al., 2006), but with coarser resolution so as to permit long simulations, and a few changes in physical parameterization noted below. The horizontal resolution is $3^{\circ} \times 3^{\circ}$ in the mid-latitudes telescoping to $3^{\circ} \times 2/3^{\circ}$ near the equator, thus capturing the critical scales of the equatorial current system. The model has 28 levels in the vertical with a top layer with a nominal thickness of 10 m, 9 layers in the upper 100 m, and bottom topography represented using partial cells so that the bottom is relatively independent of vertical resolution (Pacanowski and Gnanadesikan, 1998). Both the mixing and residual flow associated with mesoscale eddies are parameterized using diffusion coefficients as in Griffies et al. (2005a), with the difference that the maximum thickness diffusion coefficient is increased from $800\,m^2\,s^{-1}$ to $1000\,m^2\,s^{-1}$ (this was done to try to limit excessive Southern Ocean convection). As the model has coarser horizontal resolution, the lateral viscosity is increased so as to resolve the Munk layer in the western boundary.

The model uses an explicit free surface, allowing representation of real freshwater fluxes and eliminating the need for virtual fluxes of carbon dioxide associated with rigid-lid models. There is also an explicit mixed layer, the K-profile parameterization (KPP) of Large et al. (1994) that allows for convective plumes to stir up thermocline water. The overflow parameterization of Campin and Goosse (1999) was included in this run in order to maintain the stability of the Atlantic overturning and to increase the stratification in the Southern Ocean. The vertical diffusion away from the mixed layer varies between $0.15\,cm^2\,s^{-1}$ in the pycnocline and $1.2\,cm^2\,s^{-1}$ in the abyss throughout the World Ocean (in contrast with the CM2.1 models where the pycnocline diffusivity was $0.3\,cm^2\,s^{-1}$ in the polar regions). Sea ice is simulated using the GFDL

BGD
6, 10381–10446, 2009

dynamic/thermodynamic Sea Ice Simulator (SIS) model.

The surface forcing used for the model is the data product of Large and Yeager (2004) prepared for the Coordinated Ocean Reference Experiment (CORE) project (Griffies et al., 2009). The data product used here is a "climatological year" constructed from the CORE product spanning 1958–2004 with sub-monthly variability of 1959 superimposed on it. As such, it fully accounts for seasonal variations, and does not account for interannual variability. The forcing has realistic 6 h variability in wind speeds, air temperature, relative humidity and atmospheric pressure (thus permitting computation using bulk formulae of sensible and latent heat fluxes and wind stress), realistic daily variability in radiative fluxes, and realistic monthly variability in precipitation, and annual-mean runoff. Such formulations do not allow for feedbacks between evaporation and precipitation, as atmospheric relative humidity and temperature are prescribed. Thus, it is necessary to weakly restore surface salinities to prevent the thermohaline circulation from collapsing. A restoring time scale corresponding to 146 d over the top 10 m was used for the salinity, with the required corrections being applied as a surface freshwater flux.

Appendix C

Comparison of model simulations to iron fertilization observations

The four sites selected for this study were chosen because they are located in HNLC regions and because of their proximity to the sites of actual in situ iron fertilization experiments (Table C1). A distinct difference between the model iron addition simulations and the actual in situ iron fertilization experiments is the timescale and rate of deployment of the iron. In the 1× model simulations described in this paper, iron was added continuously for one month, whereas during in situ experiments iron was added over one to four patches, each lasting ~24 h and spread out over a period of up to a few weeks. The difference in the amount of iron added is also notable: ~90 g km^{-2} over

BGD
6, 10381–10446, 2009

a month in the 1× model simulations, vs. an initial ~24 h deployment of iron in in situ patches of between 1400 and 5900 g km^{-2} (Table C1). In order to be able to better compare the model simulations with the in situ iron addition experiments, we carried out an additional series of one month (1×) iron fertilization simulations with flux multiples of 5× (1×–5), 10× (1×–10) and 100× (1×–100) times the original flux of ~90 g km^{-2}, which give cumulative iron additions of ~500 g km^{-2}, 900 g km^{-2} and 9 000 g km^{-2}, respectively, thereby spanning the actual in situ iron addition experiments.

The gross biological response of model iron additions compare well with in situ iron addition experiments. In general in situ experiments have resulted in about a 10-fold increase in chlorophyll concentration, a 2-fold increase in Chl:C and a community shift from small to large phytoplankton (Table C1). The PAPA model location of 50° N 145° W, and fertilization month of May was near the 2002 SERIES (50° N 144° W, July) in situ iron addition (Boyd et al., 2005). The PAPA 1×–10 and 1×–100 model simulations obtained chlorophyll concentrations of 2.2–5.2 mg m^{-3}, Chl:C ratio increases from 0.008 to between 0.015 and 0.019 g:g, and a community composition shift from 15% large phytoplankton to between 50 and 76% large phytoplankton (Table C1). The nearby SERIES iron addition experiment had a similar response, with maximum chlorophyll concentrations of 6.3 mg m^{-3}, a doubling of the Chl:C ratio in small phytoplankton from 0.004 to 0.008 g:g, a 4-fold increase of the Chl:C ratio in large phytoplankton from 0.005 to 0.024 g:g, and a floristic shift of large phytoplankton from 26–86% (Table C1; Boyd et al., 2005; Marchetti et al., 2006). The model simulations and in situ experiments also compared well at the other three sites, where the 1×–10 model simulations at Eq-pac, Southern Ocean and Ross Sea reached a peak chlorophyll concentration of 1.4, 2.1 and 5.2 mg m^{-3}, respectively, while IronExII (Landry, 2002), SOFeX North (Lance et al., 2007) and SOFeX South (Coale et al., 2004) reported maximum chlorophyll concentrations of 3.3, 2.1 and 3.8 mg m^{-3}, respectively (Table C1).

There have been very few in situ measurements of carbon export associated with iron addition and they are limited to the Southern Ocean. Within the Antarctic Circumpolar Current, Blain et al. (2007) estimated a short term 53 000 mol C:mol Fe export

BGD
6, 10381–10446, 2009

efficiency in the upper 100 m and a 70 000 mol C:mol Fe export efficiency in the upper 200 m for a natural iron addition near the Kergulean Plateau. Blain et al. (2007) calculated a 668 000 mol C:mol Fe export efficiency for the Kergulean Plateau based on seasonal Fe and DIC inventories. Pollard et al. (2009) also calculated a seasonal export efficiency for a natural iron addition near Crozet island. Using the ^{234}Th deficit to calculate the daily carbon flux and the ^{234}Th/opal ratios to estimate the bloom duration, Pollard et al. (2009) estimated a seasonal mol C:mol Fe export efficiency of 17 200 at 100 m and 8600 at 200 m. Bishop et al. (2004) estimated an export efficiency ratio of between 10 000 and 140 000 mol C:mol Fe for the SOFeX North experiment (Coale et al., 2004). The 1×, 1×–5, 1×–10 and 1×–100 model simulations predict an export efficiency of between 168 000 and 110 000 mol C:mol Fe (Table C1). Poleward of the Southern Boundary of the Antarctic Circumpolar Current, Buesseler et al. (2004) estimated an export efficiency of 6600 mol C:mol Fe in the SOFeX South experiment (Coale et al., 2004). The 1× model suite in the Ross Sea gives export efficiencies of between 42 800 and 171 000 mol C:mol Fe (Table C1).

In both regions of the Southern Ocean, the model export efficiencies predictions were significantly higher than in situ measurements. However, the spatial and temporal time scales may play an important role in these differences. In situ observational estimates were made from carbon export measurements made below the highly dynamic patch during the enrichment and assuming no loss in iron. The model estimates an integrated global increase in export over the time period of one year. While there are no in situ export efficiencies in the North Atlantic and equatorial Pacific to compare the models to, it is noteworthy that the 4 model regions had similar export efficiencies in the 1× runs, ranging between 201 000 mol C:mol Fe at PAPA and 165 000 mol C:mol Fe at Eqpac. In all regions, additional Fe (1×–5, 10, 100) resulted in lower export efficiencies. The most precipitous drop occurred in the high latitude regions (a 4-fold drop between the 1× and 1×–100 model runs at PAPA and Ross Sea), while the EqPac and Southern Ocean regions declined more modestly.

BGD
6, 10381–10446, 2009

Acknowledgements. JLS, RDS, and MRH acknowledge support from DOE grant DE-FG02-00ER63009 and by the Carbon Mitigation Initiative supported by BP Amoco and Ford Motor Company. Comments by X. Jin were very helpful in clarifying our analysis of the fertilization efficiency. We greatly appreciate reviews by S. Henson, K. Rodgers, and M. Westley.

References

Abell, J., Emerson, S., and Renaud, P.: Distributions of TOP, TON and TOC in the North Pacific subtropical gyre: Implications for nutrient supply in the surface ocean and remineralization in the upper thermocline, J. Mar. Res., 58, 203–222, 2000.

Anderson, R. F., Ali, S., Bratdmiller, L. I., Nielsen, S. H. H., Fleisher, M. Q., Anderson, B. E., and Burckle, L. H.: Wind-driven upwelling in the Southern Ocean and the deglacial rise in atmospheric CO_2, Science, 323, 1443–1448, 2009.

Archer, D. E., Eshel, G., Winguth, A., Broecker, W., Pierreumbert, R., Tobis, M., and Jacob, R.: Atmospheric pCO_2 sensitivity to the biological pump in the ocean, Global Biogeochem. Cy., 14, 1219–1230, 2000.

Aumont, O., Maier-Reimer, E., Blain, S., and Monfray, P.: An ecosystem model of the global ocean including Fe, Si, P colimitations, Global Biogeochem. Cy., 17, 1060, doi:10.129/2001GB001745, 2003.

Aumont, O. and Bopp, L.: Globalizing results from ocean in situ iron fertilization studies, Global Biogeochem. Cy., 20, GB2017, doi:10.1029/2005GB002591, 2006.

Bakker, D. C. E., Neilsdóttir, M. C., Morris, P. J., Venables, H. J., and Watson, A. J.: The island effect and biological carbon uptake for the subatarctic Crozet Archipelago, Deep-Sea Res. Pt. II, 54, 2174–2190, 2007.

Bishop, J. K. B., Wood, T. J., Davis, R. E., and Sherman, J. T.: Robotic observations of enhanced carbon biomass and export at 55° S during SOFeX, Science, 304, 417–420, 2004.

Blain, S., Quéguiner, B., Armand, L., Belviso, S., Bombled, B., Bopp, L., Bowie, A., Brunet, C., Brussaard, C., Carlotti, F., Christaki, U., Corbiere, A., Durand, I., Ebersbach, F., Fuda, J.-L., Garcia, N., Gerringa, L., Griffiths, B., Guigue, C., Guillerm, C., Jacquet, S., Jeandel, C., Laan, P., Lefevre, D., Monaco, C. L., Malits, A., Mosseri, J., Obernosterer, I., Park, Y.-H., Picheral, M., Pondaven, P., Remenyi, T., Sandroni, V., Sarthou, G., Savoye, N., Scouarnec, L., Souhaut, M., Thuiller, D., Timmermans, K., Trull, T., Uitz, J., Beek, P. V., Veld-

huis, M., Vincent, D., Viollier, E., Vong, L., and Wagener, T.: Effect of natural iron fertilization on carbon sequestration in the Southern Ocean, Nature, 446, 1070–1075, 2007.
Bopp, L., Kohfeld, K. E., and Quéré, C. L.: Dust impact on marine biota and atmospheric CO_2 during glacial periods, Paleoceanography, 18, 1046, doi:10.1029/2002PA000810, 2003.
Boyd, P. W., Watson, A. J., Law, C. S., Abraham, E. R., Trull, T., Murdoch, R., Bakker, D. C. E., Bowie, A. R., Buesseler, K. O., Chang, H., Charette, M., Croot, P., Downing, K., Frew, R., Gall, M., Hadfield, M., Hall, J., Harvey, M., Jameson, G., LaRoche, J., Liddicoat, M., Ling, R., Maldonado, M. T., McKay, R. M., Nodder, S., Pickmere, S., Pridmore, R., Rintoul, S., Safi, K., Sutton, P., Strzepek, R., Tanneberger, K., Turner, S., Waite, A., and Zeldis, J.: A mesoscale phytoplankton bloom in the polar Southern Ocean stimulated by iron fertilization, Nature, 407, 695–702, 2000.
Boyd, P. W., Law, C. S., Wong, C. S., Nojiri, Y., Tsuda, A., Levasseur, M., Takeda, S., Rivkin, R., Harrison, P. J., Strzepek, R., Gower, J., McKay, R. M., Abraham, E., Arychuk, M., Barwell-Clarke, J., Crawford, W., Crawford, D., Hale, M., Harada, K., Johnson, K., Kiyosawa, H., Kudo, I., Marchetti, A., Miller, W., Needoba, J., Nishioka, J., Ogawa, H., Page, J., Robert, M., Saito, H., Sastri, A., Sherry, N., Soutar, T., Sutherland, N., Taira, Y., Whitney, F., Wong, S. K. E., and Yoshimura, T.: The decline and fate of an iron-induced subarctic phytoplankton bloom, Nature, 428, 549–553, 2004.
Boyd, P. W., Strzepek, R., Takeda, S., Jackson, G., C. S. W., McKay, R. M., Law, C., Kiyosawa, H., Saito, H., Sherry, N., J. K., Gower, J., and Ramaiah, N.: The evolution and termination of an iron-induced mesoscale bloom in the northeast subarctic Pacific, Limnol. Oceanogr., 50, 1872–1886, 2005.
Boyd, P. W., Jickells, T., Law, C. S., Blain, S., Boyle, E. A., Buesseler, K. O., Coale, K. H., Cullen, J. J., de Baar, H. J. W., Follows, M., Harvey, M., Lancelot, C., Levasseur, M., Owens, N. P. J., Pollard, R., Rivkin, R. B., Sarmiento, J., Schoemann, V., Smetacek, V., Takeda, S., Tsuda, A., Turner, S., and Watson, A. J.: Mesoscale iron enrichment experiments 1993–2005: synthesis and future directions, Science, 315, 612–617, 2007.
Buesseler, K. O. and Boyd, P. W.: Will ocean fertilization work?, Science, 300, 67–68, 2003.
Buesseler, K. O., Andrews, J. E., Pike, S. M., and Charette, M. A.: The effects of iron fertilization on carbon sequestration in the Southern Ocean, Science, 304, 414–417, 2004.
Buesseler, K. O., Doney, S. C., Karl, D. M., Boyd, P. W., Caldeira, K., Chai, F., Coale, K. H., de Baar, H. J. W., Falkowski, P. G., Johnson, K. S., Lampitt, R. S., Michaels, A. F., Naqvi, S. W. A., Smetacek, V., Takeda, S., and Watson, A. J.: Ocean iron fertilization-moving

forward in a sea of uncertainty, Science, 319, 162, 2008.
Campin, J. M. and Goosse, H.: Parameterization of density-driven downsloping flow for a coarse-resolution model in z-coordinate, Tellus, 51A, 412–430, 1999.
Chisholm, S. W., Falkowski, P. G., and Cullen, J. J.: Dis-crediting ocean fertilization, Science, 294, 309–310, 2001.
Coale, K. H., Johnson, K. S., Fitzwater, S. E., Gordon, R. M., Tanner, S., Chavez, F. P., Ferioli, L., Sakamoto, C., Rogers, P., Millero, F., Steinberg, P., Nightingale, P., Cooper, D., Cochlan, W. P., Landry, M. R., Constantinou, J., Rollwagen, G., Trasvina, A., and Kudela, R.: A massive phytoplankton bloom induced by an ecosystem-scale iron fertilization experiment in the equatorial Pacific Ocean, Nature, 383, 495–501, 1996.
Coale, K. H., Johnson, K. S., Chavez, F. P., Buesseler, K. O., Barber, R. T., Brzezinski, M. A., Cochlan, W. P., Millero, F. J., Falkowski, P. G., Bauer, J. E., Wanninkhof, R. H., Kudela, R. M., Altabet, M. A., Hales, B. E., Takahashi, T., Landry, M. R., Bidigare, R. R., Wang, X., Chase, Z., Strutton, P. G., Friederich, G. E., Gorbunov, M. Y., Lance, V. P., Hilting, A. K., Hiscock, M. R., Demarest, M., Hiscock, W. T., Sullivan, K. F., Tanner, S. J., Gordon, R. M., Hunter, C. N., Elrod, V. A., Fitzwater, S. E., Jones, J. L., Tozzi, S., Koblizek, M., Roberts, A. E., Herndon, J., Brewster, J., Ladizinsky, N., Smith, G., Cooper, D., Timothy, D., Brown, S. L., Selph, K. E., Sheridan, C. C., Twining, B. S., and Johnson, Z. I.: Southern Ocean iron enrichment experiment: carbon cycling in high- and low-Si water, Science, 304, 408–414, 2004.
Cochlan, W. P., Bronk, D. A., and Coale, K. H.: Trace metals and nitrogenous nutrition of Antarctic phytoplankton: experimental observations in the Ross Sea, Deep-Sea Res. Pt. II, 49, 3365–3390, 2002.
de Baar, H. J. W., Boyd, P. W., Coale, K. H., Landry, M. R., Tsuda, A., Assmy, P., Bakker, D. C. E., Bozek, Y., Barber, R. T., Brzezinski, M. A., Buesseler, K. O., Boyé, M., Croot, P. L., Gervais, F., Gorbunov, M. Y., Harrison, P. J., Hiscock, W. T., Laan, P., Lancelot, C., Law, C. S., Levasseur, M., Marchetti, A., Millero, F. J., Nishioka, J., Nojiri, Y., van Oijen, T., Riebesell, U., Rijkenberg, M. J. A., Saito, H., Takeda, S., Timmrmans, K. R., Veldhuis, M. J. W., Waite, A. M., and Wong, C. S.: Synthesis of iron fertilization experiments: from the Iron Age in the Age of Elightenment, J. Geophys. Res., 110, C09S16, doi:10.1029/2004JC002601, 2005.
Dunne, J., Armstrong, R., Gnanadesikan, A., and Sarmiento, J.: Empirical and mechanistic models for the particle export ratio, Global Biogeochem. Cy., 19, GB4026, doi:4010.1029/2004GB002390, 2005.
Dutkiewicz, S., Follows, M. J., and Parekh, P.: Interactions of the iron and phospho-

rus cycles: a three-dimensional model study, Global Bilogeochem. Cy., 19, GB1021, doi:10.1029/2004GB002342, 2005.
Dutkiewicz, S., Follows, M. J., Heimbach, P., and Marshall, J.: Controls on ocean productivity and air-sea carbon flux: an adjoint model sensitivity study, Geophys. Res. Lett., 33, L02603, doi:10.1029/2005GL024987, 2006.
Frost, B. W. and Franzen, N. C.: Grazing and iron limitation in the control of phytoplankton stock and nutrient concentration: a chemostat analogue of the Pacific equatorial upwelling zone, Mar. Ecol.-Prog. Ser., 83, 291–303, 1992.
Fung, I., Meyn, S., Tegen, I., Doney, S., John, J., and Bishop, J.: Iron supply and demand in the upper ocean, Global Biogeochem. Cy., 14, 281–295, 2000.
Galbraith, E. D., Gnanadesikan, A., Dunne, J. P., and Hiscock, M. R.: Regional impacts of iron-light colimitation in a global biogeochemical model, Biogeosciences Discuss., 6, 7517–7564, 2009, http://www.biogeosciences-discuss.net/6/7517/2009/.
Gall, M. P., Boyd, P. W., Hall, J., Safi, K. A., and Chang, H.: Phytoplankton processes. Part 1: Community structure during the Southern Ocean Iron RElease Experiment (SOIREE), Deep-Sea Res. Pt. II, 48, 2551–2570, 2001.
Garcia, H. E., Locarnini, R. A., Boyer, T. P., and Antonov, J. I.: World Ocean Atlas 2005, Volume 4: Nutrients (phosphate, nitrate, silicate), in: NOAA Atlas NESDIS 64, edited by: Levitus, S., US Government Printing Office, Washington, DC, 396 pp., 2006.
Geider, R. J., MacIntyre, H. L., and Kana, T. M.: A dynamic model of phytoplankton growth and acclimation: responses of the balanced growth rate and chlrophyll-*a*: carbon ratio to light, nutrient-limitation and temperature, Mar. Ecol.-Prog. Ser., 148, 187–200, 1997.
Gervais, F., Riebesell, U., and Gorbunov, M. Y.: Changes in primary productivity and chlorophyll a in response to iron fertlization in the Southern Polar Frontal Zone, Limnol. Oceanogr., 47, 1324–1335, 2002.
Ginoux, P., Chin, M., Tegen, I., Prospero, J. M., Holben, B., Dubovik, O., and Lin, S. J.: Sources and distributions of dust aerosols simulated with the GOCART model, J. Geophys. Res.-Atmos., 106, 20255–20273, 2001.
Gnanadesikan, A., Slater, R. D., Gruber, N., and Sarmiento, J. L.: Oceanic vertical exchange and new production: a comparison between models and observations, Deep-Sea Res. Pt. II, 49, 363–401, 2002.
Gnanadesikan, A., Sarmiento, J. L., and Slater, R. D.: Effects of patchy ocean fertilization

on atmospheric carbon dioxide and biological production, Global Biogeochem. Cy., 17, doi:10.1029/2002GB001940, 2003.
Gnanadesikan, A., Dixon, K. W., Griffies, S. M., et al.: GFDL's CM2 global coupled climate models, J. Climate, 19, 675–697, 2006.
Gnanadesikan, A. and Marinov, I.: Export is not enough: Nutrient cycling and carbon, Mar. Ecol.-Prog. Ser., 364, 289–294, 2008.
Griffies, S. M., Gnanadesikan, A., Dixon, K. W., Dunne, J. P., Gerdes, R., Harrison, M. J., Rosati, A., Russell, J. L., Samuels, B. L., Spelman, M. J., Russell, J., Winton, M., and Zhang, R.: Formulation of an ocean model for global climate simulations, Ocean Sci., 1, 45–79, 2005a, http://www.ocean-sci.net/1/45/2005/.
Griffies, S. M., Harrison, M. J., Pacanowski, R. C., and Rosati, A.: A technical guide to MOM4, GFDL Ocean Group Technical Report No. 5, NOAA/Geophysical Fluid Dynamics Laboratory, Princeton, 2005b.
Griffies, S. M., Biastoch, A., Böning, C., Bryan, F., Danabasoglu, G., Chassignet, E. P., England, M. H., Gerdes, R., Haak, H., Hallberg, R. W., et al.: Coordinated ocean-ice reference experiments (COREs), Ocean Model., 26, 1–46, 2009.
Hiscock, M. R., Lance, V. P., Apprill, A, Bidigare, R. R, Johnson, Z. I., Mitchell, B. G. Smith, W. O., and Barber, R. T.: Photosynthetic maximum quantum yield increases are an essential component of the Southern Ocean phytoplankton response to iron, P. Natl. Acad. Sci. USA, 105, 4775–4780, 2008.
Hoffmann, L. J., Peeken, I., Lochte, K., Assmy, P., and Veldhuis, M.: Different reactions of Southern Ocean phytoplankton size classes to iron fertilization, Limnol. Oceanogr., 51, 1217–1229, 2006.
Jin, X. and Gruber, N.: Offsetting the radiative benefit of ocean iron fertilization by enahncing N_2O emissions, Geophys. Res. Lett., 30, 2249, 2003.
Jin, X., Gruber, N., Frenzel, H., Doney, S. C., and McWilliams, J. C.: The impact on atmospheric CO_2 of iron fertilization induced changes in the ocean's biological pump, Biogeosciences, 5, 385–406, 2008, http://www.biogeosciences.net/5/385/2008/.
Johnson, K. S., Gordon, R. M., and Coale, K. H.: What controls dissolved iron concentrations in the world ocean?, Mar. Chem., 57, 137–161, 1997.
Joos, F., Sarmiento, J. L., and Siegenthaler, U.: Estimates of the effect of Southern Ocean iron

fertilization on atmospheric CO_2 concentrations, Nature, 349, 772–774, 1991.
Jouandet, M. P., Blain, S., Metzl, N., Brunet, C., Trull, T. W., and Obernosterer, I.: A seasonal carbon budget for a naturally iron-fertilzed bloom over the Kerguelen Plateau in the Southern Ocean, Deep-Sea Res. Pt. II, 55, 856–867, 2008.
Knox, F. and McElroy, M.: Changes in atmospheric CO_2, influence of marine biota at high latitudes, J. Geophys. Res., 89, 4629–4637, 1984.
Kurz, K. D. and Maier-Reimer, E.: Iron fertilization of the austral ocean – the Hamburg model assessment, Global Biogeochem. Cy., 7, 229–244, 1993.
Lance, V. P., Hiscock, M. R., Hilting, A. K., Stuebe, D. A., Bidigare, R. R., Smith Jr., W. O., and Barber, R. T.: Primary productivity, diferential size fraction and pigment composition responses in two Southern Ocean in situ iron enrichments, Deep-Sea Res. Pt. I, 54, 747–773, 2007.
Landry, M. R.: Integrating classical and microbial food web concepts: evolving views from the open-ocean tropical Pacific, Hydrobiologia, 480, 29–39, 2002.
Large, W. G., McWilliams, J. C., and Doney, S. C.: Oceanic vertical mixing: a Review and a model with a nonlocal boundary layer, Rev. Geophys., 32, 363–403, 1994.
Large, W. G. and Yeager, S. G.: Diurnal to decadal global forcing for ocean and sea-ice models: the data sets and flux climatologies, Tech. Rep. NCAR/TN-460_STR, National Center for Atmospheric Research, Boulder, CO, 2004.
Law, C. S., Crawford, W. R., Smith, M. J., Boyd, P. W., Wong, C. S., Nojiri, Y., Robert, M., Abraham, E. R., Johnson, W. K., Forsland, V., and Arychuk, M.: Patch evolution and the biogeochemical impact of entrainment during a mesoscale iron enrichment in the subarctic Pacific, Deep-Sea Res. Pt. II, 53, 2012–2033, 2006.
Letelier, R. M. and Karl, D. M.: Trichodesmium spp. physiology and nutrient fluxes in the North Pacific subtropical gyre, Aquatic Microbial Ecology, 15, 265–276, 1998.
Marchetti, A., Sherry, N. D., Kiyosawa, H., Tsuda, A., and Harrison, P. J.: Phytoplankton processes during a mesoscale iron enrichment in the NE subarctic Pacific: Part I – biomass and assemblage, Deep-Sea Res. Pt. II, 53, 2095–2113, 2006.
Marinov, I., Gnanadesikan, A., Toggweiler, J. R., and Sarmiento, J. L.: The Southern Ocean biogeochemical divide, Nature, 441, 964–967, 2006.
Marinov, I., Follows, M., Gnanadesikan, A., Sarmiento, J. L., and Slater, R. D.: How does ocean biology affect atmospheric pCO_2: theory and models, J. Geophys. Res., 113, C07032, doi:10.1029/2007JC004598, 2008.

BGD
6, 10381–10446, 2009

Martin, J. H., Knauer, G. A., Karl, D. M., and Broenkow, W. W.: VERTEX: carbon cycling in the northeast Pacific, Deep-Sea Res., 34, 267–285, 1987.
Martin, J. H.: Glacial-interglacial CO_2 change: the iron hypothesis, Paleoceanography, 5, 1–13, 1990.
Martin, J. H., Fitzwater, S. E., and Gordon, R. M.: Iron deficiency limits phytoplankton growth in Antarctic waters, Global Biogeochem. Cy., 4, 5–12, 1990a.
Martin, J. H., Gordon, R. M., and Fitzwater, S. E.: Iron in Antarctic waters, Nature, 345, 156–158, 1990b.
Martin, J. H., Coale, K. H., Johnson, K. S., Fitzwater, S. E., Gordon, R. M., Tanner, S. J., Hunter, C. N., Elrod, V. A., Nowicki, J. L., Coley, T. L., Barber, R. T., Lindley, S., Watson, A. J., Vanscoy, K., Law, C. S., Liddicoat, M. I., Ling, R., Stanton, T., Stockel, J., Collins, C., Anderson, A., Bidigare, R., Ondrusek, M., Latasa, M., Millero, F. J., Lee, K., Yao, W., Zhang, J. Z., Friederich, G., Sakamoto, C., Chavez, F., Buck, K., Kolber, Z., Greene, R., Falkowski, P., Chisholm, S. W., Hoge, F., Swift, R., Yungel, J., Turner, S., Nightingale, P., Hatton, A., Liss, P., and Tindale, N. W.: Testing the iron hypothesis in ecosystems of the equatorial Pacific Ocean, Nature, 371, 123–129, 1994.
Matear, R. and Elliott, B.: Enhancement of oceanic uptake of anthropogenic carbon by macronutrient fertilization, J. Geophys. Res., 109, C04001, doi:1029/2000JC000321, 2004.
Matsumoto, K.: Model simulations of carbon sequestration in the northwest Pacific by patch fertilization, J. Oceanogr., 62, 887–902, 2006.
Middelburg, J. J., Soetaert, K., Herman, P. M. J., and Heip, C. H. R.: Denitrification in marine sediments: a model study, Global Biogeochem. Cy., 10, 661–673, 1996.
Mongin, M., Nelson, D. M., Pondaven, P., and Tréguer, P.: Potential phytoplankton response to iron and stratification changes in the Southern Ocean based on a flexible-composition phytoplankton model, Global Biogeochem. Cy., 21, GB4020, doi:4010.1029/2007GB002972, 2007.
Moore, J. K. and Doney, S. C.: Iron availability limits the ocean nitrogen inventory stabilizing feedbacks between marine denitrification and nitrogen fixation, Global Biogeochem. Cy., 21, GB2001, doi:10.1029/2006GB002762, 2007.
Moore, J. K., Doney, S. C., Glover, D. M., and Fung, I. Y.: Iron cycling and nutrient-limitation patterns in surface waters of the World Ocean, Deep-Sea Res. Pt. II, 49, 463–507, 2002a.
Moore, J. K., Doney, S. C., Kleypas, J. A., Glover, D. M., and Fung, I. Y.: An intermediate complexity marine ecosystem model for the global domain, Deep-Sea Res. Pt. II, 49, 463–

507, 2002b.
Orr, J. C. and Sarmiento, J. L.: Potential of marine macroalgae as a sink for CO_2: constraints from a 3-D general circulation model of the global ocean, Water Air Soil Poll., 64, 405–421, 1992.
Oschlies, A.: Impact of atmospheric and terrestrial CO_2 feedbacks on fertilization-induced marine carbon uptake, Biogeosciences, 6, 1603–1613, 2009, http://www.biogeosciences.net/6/1603/2009/.
Pacanowski, R. C. and Gnanadesikan, A.: Transient response in a z-level ocean model with bottom topography resolved using the method of partial cells, Mon. Weather Rev., 104, 3248–3270, 1998.
Peng, T. H. and Broecker, W. S.: Dynamic limitations on the Antarctic iron fertilization strategy, Nature, 349, 227–229, 1991.
Pollard, R. T., Salter, I., Sanders, R. J., Lucas, M. I., Moore, C. M., Mills, R. A., Statham, P. J., Allen, J. T., Baker, A. R., Bakker, D. C. E., Charette, M. A., Fielding, S., Fones, G. R., French, M., Hickman, A. E., Holland, R. J., Hughes, J. A., Jickells, T. D., Lampitt, R. S., Morris, P. J., Nédélec, F. H. N., M, Planquette, H., Popova, E. E., Poulton, A. J., Read, J. F. S., S, Smith, T., Stinchcombe, M., Taylor, S., Thomalla, S., Venables, H. J., Williamson, R., and Zubkov, M. V.: Southern Ocean deep-water carbon export enhanced by natural iron fertilization, Nature, 457, 577–580, 2009.
Sarmiento, J. L. and Toggweiler, J. R.: A new model for the role of the oceans in determining atmospheric pCO_2, Nature, 308, 621–624, 1984.
Sarmiento, J. L. and Orr, J. C.: Three-dimensional simulations of the impact of Southern Ocean nutrient depletion on atmospheric CO_2 and ocean chemistry, Limnol. Oceanogr., 36, 1928–1950, 1991.
Sarmiento, J. L. and Gruber, N.: Ocean Biogeochemical Dynamics, Princeton University Press, Princeton, 2006.
Schiermeier, Q.: Climate change: the oresmen, Nature, 421, 109–110, 2003.
Schneider, B., Bopp, L., Gehlen, M., Segschneider, J., Frölicher, T. L., Cadule, P., Friedlingstein, P., Doney, S. C., Behrenfeld, M. J., and Joos, F.: Climate-induced interannual variability of marine primary and export production in three global coupled climate carbon cycle models, Biogeosciences, 5, 597-614, 2008, http://www.biogeosciences.net/5/597/2008/.
Sharada, M. K., Yajnik, K. S., and Swathi, P. S.: Evaluation of six relations of the kinetics of

uptake by phytoplankton in multi-nutrient environment using JGOFS experimental results, Deep-Sea Res. Pt. II, 52, 1892–1909, 2005.
Shepherd, J.: Geoengineering the Climate: Science, Governance and Uncertainty, RS Policy document 10/09, The Royal Society, London, 1–82, 2009.
Siegenthaler, U. and Wenk, T.: Rapid atmospheric CO_2 variations and ocean circulation, Nature, 308, 624–626, 1984.
Sigman, D. M. and Boyle, E. A.: Glacial/interglacial variations in atmospheric carbon dioxide, Nature, 407, 859–869, 2000.
Strong, A., Chisholm, S. Miller, C., and Cullen, J.: Ocean fertilization: time to move on, Nature, 461, 347–348, 2009.
Sunda, W. G. and Huntsman, S. A.: Interrelated influence of iron, light and cell size on marine phytoplankton growth, Nature, 390, 389–392, 1997.
Sunda, W. G.: Bioavailability and bioaccumulation of iron in the sea, in: The Biogeochemistry of Iron in Seawater, edited by: Turner, D. R. and Hunter, K. A., John Wiley & Sons, Ltd., Chichester, 41–84, 2001.
Tagliabue, A. and Arrigo, K. R.: Processes governing the supply of iron to phytoplankton in stratified seas, J. Geophys. Res., 111, C06019, doi:10.1029/2005JC003363, 2006.
Tagliabue, A., Bopp, L., and Aumont, O.: Ocean biogeochemistry exhibits contrasting responses to a large scale reduction in dust deposition, Biogeosciences, 5, 11–24, 2008, http://www.biogeosciences.net/5/11/2008/.
Takeda, S. and Tsuda, A.: An in situ iron-enrichment experiment in the western subarctic Pacific (SEEDS): introduction and summary, Prog. Oceanogr., 64, 95–109, 2005.
Tsuda, A., Takeda, S., Saito, H., Nishioka, J., Nojiri, Y., Kudo, I., Kiyosawa, H., Shiomoto, A., Imai, K., Ono, T., Shimamoto, A., Tsumune, D., Yoshimura, T., Aono, T., Hinuma, A., Kinugasa, M., Suzuki, K., Sohrin, Y., Noiri, Y., Tani, H., Deguchi, Y., Tsurushima, N., Ogawa, H., Fukami, K., Kuma, K., and Saino, T.: A mesoscale iron enrichment in the western Subarctic Pacific induces a large centric diatom bloom, Science, 300, 958–961, 2003.
Zeebe, R. E. and Archer, D.: Feasibility of ocean fertilization and its impacts on future atmospheric CO_2 levels, Geophys. Res. Lett., 32, L09703, doi:09710.01029/02005GL022449, 2005.

Table 1. Results of regional iron fertilization simulations in which the effect of iron fertilization is assumed to be continuous for a period of 100 yr. The total amount of carbon in the atmosphere-ocean system is preserved. In other words, as CO_2 is removed from the atmosphere, the CO_2 drops below its control value of 278 ppm, which permits CO_2 to escape from the ocean in regions that are not being fertilized. These simulations provide an upper limit for how much CO_2 could be removed by massive regional iron fertilization. Model drift is corrected for by subtracting a control simulation in which the total amount of carbon in the system is also fixed.

Region of nutrient depletion or iron fertilization	CO_2 drawdown (ppm)	
	KVHISOUTH[a]	This model[b]
Southern Ocean (90° S–30° S)	39.0	35.3
Tropics (18° S–18° N)	4.6	9.5
North Atlantic (30° S–80° N)	5.1	0.5
North Pacific (30° N–67° N)	3.5	3.2
Global	52.1	41.8

[a] KVHISOUTH is described in Gnanadesikan et al. (2002). Surface nutrient biogeochemistry is simulated in this model by restoring model predicted surface nutrients to observations except in the region of nutrient depletion where nutrients are forced to zero. The response of this model is typical of the response of a wide range of similar such models.

[b] In this particular simulation, where we wanted to see what would happen if iron limitation were eliminated entirely, iron fertilization was simulated by turning off iron limitation in the specified region, which essentially amounted to adding an infinite amount of iron. Note that the control scenario of the model used in this study has too high nutrients in the tropics and too low in the Southern Ocean, which contributes to enhancing its response in the tropics and muting it in the Southern Ocean relative to KVHISOUTH, where nutrients are forced towards observations in the control scenario.

BGD
6, 10381–10446, 2009

Table 2. Patch locations and fertilization time in the 1×, 10×, and 100× simulations.

Name	Location	Number of model grid cells	Patch size (10^3 km^2)	Month of fertilization
PAPA (North Pacific)	50.0° N, 145° W	2	72.3	May
Equatorial Pacific	3.5° S, 104° W	1	106.5	Sep
Southern Ocean	58.5° S, 171° W	2	116.3	Oct
Ross Sea	76.0° S, 176° W	4	103.9	Jan

BGD
6, 10381–10446, 2009

Table 3. Nitrogen budget at the iron fertilization sites in the 1200× scenario.

Field	N change over 100 yr (Tmol/100 yr) PAPA	Equatorial Pacific	Southern Ocean	Ross Sea
N_2 fixation	0.194	0.837	0.125	0.002
Sed denitrification	0.000	−0.003	−0.003	0.016
Water Col Denitrification	−0.337	4.827	−0.269	−0.014
ΔNO_3	0.520	−3.960	0.267	−0.039

BGD
6, 10381–10446, 2009

Table 4. Effectiveness and efficiency of CO_2 uptake from the atmosphere.

(a) Effectiveness=cumulative CO_2 uptake (Tg C)

	Year 10				Year 50				Year 100			
	PAPA	Eq. Pac.	S. Ocean	Ross Sea	PAPA	Eq Pac.	S. Ocean	Ross Sea	PAPA	Eq. Pac.	S. Ocean	Ross Sea
1×	0.16	0.17	0.30	0.35	0.03	0.04	0.18	0.34	0.08	0.03	0.14	0.39
10×	2.13	2.25	3.33	3.55	0.40	0.71	1.71	3.35	0.38	0.52	1.24	3.12
100×	2.13	2.25	3.33	3.55	4.93	5.98	12.1	17.2	6.76	9.03	19.2	33.5
1200×	16.8	30.8	37.4	12.1	47.8	79.1	138.0	66.8	69.4	117.0	222.0	136.0

(b) Efficiency=C:Fe mol ratio of CO_2 uptake to iron addition ($\times 10^5$)

	Year 10				Year 50				Year 100			
	PAPA	Eq. Pac.	S. Ocean	Ross Sea	PAPA	Eq Pac.	S. Ocean	Ross Sea	PAPA	Eq. Pac.	S. Ocean	Ross Sea
1×	1.10	0.83	1.32	1.72	0.20	0.17	0.77	1.66	0.52	0.14	0.62	1.88
10×	1.49	1.06	1.44	1.70	0.28	0.34	0.74	1.61	0.26	0.25	0.54	1.50
100×	1.49	1.06	1.44	1.70	0.69	0.57	1.04	1.65	0.47	0.43	0.83	1.61
1200×	0.98	1.21	1.35	0.49	0.55	0.62	1.00	0.54	0.40	0.46	0.80	0.55

BGD
6, 10381–10446, 2009

Table 5. Atmospheric reservoir effect. The table shows the ratio of a model with an atmospheric reservoir to the same simulation without a reservoir. The Equatorial Pacific 1× result is not trustworthy because the cumulative uptake is near 0 at 100 yr.

Iron flux multiple	1×		10×		100×		1200×	
Time of analysis	10 yr	100 yr	10 yr	100 yr	10 yr	100 yr	10 yr	100 yr
PAPA	0.58	0.24	0.79	0.26	0.79	0.45	0.80	0.47
Equatorial Pacific	0.59	(1.87)	0.81	0.27	0.81	0.48	0.80	0.48
Southern Ocean	0.67	0.30	0.81	0.31	0.81	0.50	0.80	0.51
Ross Sea	0.69	0.31	0.80	0.40	0.80	0.53	0.81	0.53

BGD
6, 10381–10446, 2009

Table C1. Comparison of iron fertilization simulation results to observations at nearby purposeful or natural iron fertilization experimental sites or locations with similar biogeochemical properties. Note: in the following, KEOPS is the Kerguelen ocean and plateau compared study, EIFEX is the European Iron Fertilization Experiment, and SOFeX is the Southern Ocean iron experiment.

Iron Ex	Type	Location	Time	Iron addition	Iron addition to initial patch ($g\,km^{-2}$)	Max dissolved Fe (nM)	Mean Chl ambient ($mg\,m^{-3}$)	Max Chl (+Fe) ($mg\,m^{-3}$)	Mean ambient Chl:C (g:g)	Max Chl:C (+Fe)	Mean % Large Phyto	% Large Phyto (+Fe)	Delta carbon export, 100 m (+Fe)	Carbon export efficiency, 100 m (+Fe) mol C:mol Fe	References
PAPA	this study	50° N 145° W	May	6783 kg	94	0.003	0.48	0.90	0.008	0.011	15%	22%	0.29 Tg	201 000	one month 1× (1×)
PAPA	this study	50° N 145° W	May	33 920 kg	469	0.022	0.48	1.69	0.008	0.014	15%	39%	1.1 Tg	157 000	one month 5x(1×–5)
PAPA	this study	50° N 145° W	May	67 830 kg	940	0.066	0.48	2.27	0.008	0.015	15%	50%	2.0 Tg	137 000	one month 10× (1×–10)
PAPA	this study	50° N 145° W	May	678 300 kg	9400	2.52	0.48	5.22	0.008	0.019	15%	76%	8.6 Tg	58 700	one month 100× (1×–100)
SEEDS I	in situ Fe addition	48.5° N 165° E	18 Jul –1 Aug 2001	350 kg	4400	2.9	0.76	21.8	0.005 Chl:POC	0.015 Chl:POC	36%	95%	n/a	n/a	Takeda and Tsuda (2005), Marchetti et al. (2006), Law et al. (2006)
SERIES	in situ Fe addition	50° N 144° W	11 Jul –4 Aug 2002	490 kg	5900	>1	0.35	6.3	0.004 for <5 um 0.005 for >5 um	0.008 for <5 um 0.024 for >5 um	26%	86%	n/a	n/a	Boyd et al. (2005), Marchetti et al. (2006)
EqPac	this study	3.5° S 104° W	Sep	9 670 kg	91	0.004	0.46	0.65	0.011	0.014	15%	23%	0.34 Tg	165 000	one month 1× (1×)
EqPac	this study	3.5° S 104° W	Sep	48 350 kg	454	0.013	0.46	1.02	0.011	0.015	15%	38%	1.5 Tg	146 000	one month 5× (1×–5)
EqPac	this study	3.5° S 104° W	Sep	96 700 kg	910	0.030	0.46	1.40	0.011	0.017	15%	48%	2.8 Tg	137 000	one month 10× (1×–10)
EqPac	this study	3.5° S 104° W	Sep	967 000 kg	9100	1.043	0.46	4.56	0.011	0.024	15%	77%	22 Tg	107 000	one month 100× (1×–100)
IronEX I	in situ Fe addition	5° S 90° W	Oct, 1993	450 kg	n/a	~4	0.24	0.65	0.019	0.026	n/a	n/a	n/a	n/a	Martin et al. (1994)
IronEX I	Galapogos plume	1° S 91° W	Oct, 1993	outside plume (0.06 nM Fe)	n/a	1.3	0.24	0.7	n/a	n/a	n/a	n/a	n/a	n/a	Martin et al. (1994)
IronEX II	in situ Fe addition	3.5° S 104° W	29 May –16 Apr, 1995	450 kg	3100	2	0.21	3.3	0.007	0.014	>18 um accounted for 6% of PP_{eu}	>18 um accounted for 65% of PP_{eu}	n/a	n/a	Lindley (personal communication), Landry (2002)

BGD
6, 10381–10446, 2009

Table C1. Continued.

Iron Ex	Type	Location	Time	Iron addition	Iron addition to initial patch ($g\,km^{-2}$)	Max dissolved Fe (nM)	Mean Chl ambient ($mg\,m^{-3}$)	Max Chl (+Fe) ($mg\,m^{-3}$)	Mean ambient Chl:C (g:g)	Max Chl:C (+Fe)	Mean % Large Phyto	% Large Phyto (+Fe)	Delta carbon export, 100 m (+Fe)	Carbon export efficiency, 100 m (+Fe) mol C:mol Fe	References
Southern Ocean	this study	60° S 179° W	Oct	10 915 kg	94	0.014	0.59	0.91	0.012	0.018	36%	51%	0.39 Tg	168 000	one month 1× (1×)
Southern Ocean	this study	60° S 179° W	Oct	54 570 kg	469	0.017	0.59	1.32	0.012	0.018	36%	51%	1.8 Tg	152 000	one month 5× (1×–5)
Southern Ocean	this study	60° S 179° W	Oct	109,150 kg	940	0.035	0.59	2.11	0.012	0.019	36%	64%	3.5 Tg	151 000	one month 10× (1×–10)
Southern Ocean	this study	60° S 179° W	Oct	1 091 500 kg	9400	0.846	0.59	9.16	0.012	0.028	36%	87%	26 Tg	110 000	one month 100× (1×–100)
SOFeX North	in situ Fe addition	56° S 172° W	10 Jan–10 Feb 2002	1400–1712 kg	2800	1.2	0.17	2.1	n/a	n/a	6% >20 um	66% >20 um	120–1170 $mmol\,m^{-2}\,d^{-1}$	10 000–140 000	Bishop et al. (2004), Lance et al. (2007)
KEOPS	natural Fe addition (short term ^{234}Th deficit)	50° S 72° E	19 Jan –13 Feb 2005	2.04×10^{-4} $mmol\,m^{-2}\,d^{-1}$	297	0.09 (0.19–0.51 at 500 m)	0.2	3	n/a	n/a	>10 um accounted for 34% of PP_{eu}	>10 um accounted for 79% of PP_{eu}	10.8 $mmol\,m^{-2}\,d^{-1}$	53 000	Blain et al. (2007)
KEOPS	natural Fe addition (seasonal inventory estimate)	50° S 72° E	Seasonal inventory estimate	4.96×10^{-3} $mmol\,m^{-2}$	n/a	n/a	n/a	n/a	n/a	n/a	n/a	n/a	3317 $mmol\,m^{-2}$	668 000	Blain et al. (2007)
Crozet	natural Fe addition (^{234}Th deficit and ^{234}Th/opal ratios)	45° S 50° E	Seasonal estimate (2004–2005)	0.039 $mmol\,m^{-2}$	n/a	n/a	n/a	6 $mg\,m^{-3}$	n/a	n/a	n/a	n/a	670 $mmol\,m^{-2}$	17 200	Pollard et al. (2009)
SOIREE	in situ Fe addition	61° S 140° E	9–22 Feb 1999	1750 kg	n/a	~2.5	0.2	2.3	<0.010 for bulk 0.008 for >20 um	0.025 for bulk 0.029 for >20 um	30%	50%	n/a	n/a	Marchetti et al. (2006), Boyd et al. (2000), Gall et al. (2001)
EisenEx	in situ Fe addition	48° S 21° E	6–29 Nov 2000	2350 kg	n/a	n/a	0.5	2.8	n/a	n/a	10%	43%	n/a	n/a	Gervais et al. (2002)
EIFEX	in situ Fe addition	50° S 2° E	21 Jan –25 Mar 2004	2820 kg	n/a	~2	0.54	2.85	0.006 Chl:POC	0.018 Chl:POC	18%	46%	n/a	n/a	Hoffmann et al. (2006)

BGD
6, 10381–10446, 2009

Table C1. Continued.

Iron Ex	Type	Location	Time	Iron addition	Iron addition to initial patch ($g\,km^{-2}$)	Max dissolved Fe (nM)	Mean Chl ambient ($mg\,m^{-3}$)	Max Chl (+Fe) ($mg\,m^{-3}$)	Mean ambient Chl:C (g:g)	Max Chl:C (+Fe)	Mean % Large Phyto	% Large Phyto (+Fe)	Delta carbon export, 100 m (+Fe)	Carbon export efficiency, 100 m (+Fe) mol C:mol Fe	References
Ross Sea	this study	76° S 176° W	Jan	9793 kg	94	0.011	0.75	1.15	0.008	0.013	31%	42%	0.36 Tg	171 000	one month 1× (1×)
Ross Sea	this study	76° S 176° W	Jan	48 963 kg	469	0.070	0.75	3.16	0.008	0.016	31%	73%	1.8 Tg	167 000	one month 5× (1×–5)
Ross Sea	this study	76° S 176° W	Jan	97 930 kg	940	0.372	0.75	5.19	0.008	0.021	31%	81%	3.0 Tg	140 000	one month 10× (1×–10)
Ross Sea	this study	76° S 176° W	Jan	979 300 kg	9400	8.04	0.75	10.11	0.008	0.023	31%	87%	9.0 Tg	42 800	one month 100× (1×–100)
SOFeX South	in situ Fe addition	66° S 172° W	24 Jan–5 Feb 2002	1260 kg	1400	0.7	0.41	3.8	0.004 Chl:POC	0.010 Chl:POC	50% of biomass >20 um	58% of biomass >20 um	1 800 000 kg	6600	Buesseler et al. (2004), Coale et al. (2004), Lance et al. (2007)
JGOFS – Blue	on-deck incubation	74° S 176° W	26 Jan–7 Feb 1997	from 0.03 to 1.5 nM	n/a	1.5	0.52	~6	n/a	n/a	n/a	n/a	n/a	n/a	Cochlan et al. (2002)

BGD
6, 10381–10446, 2009

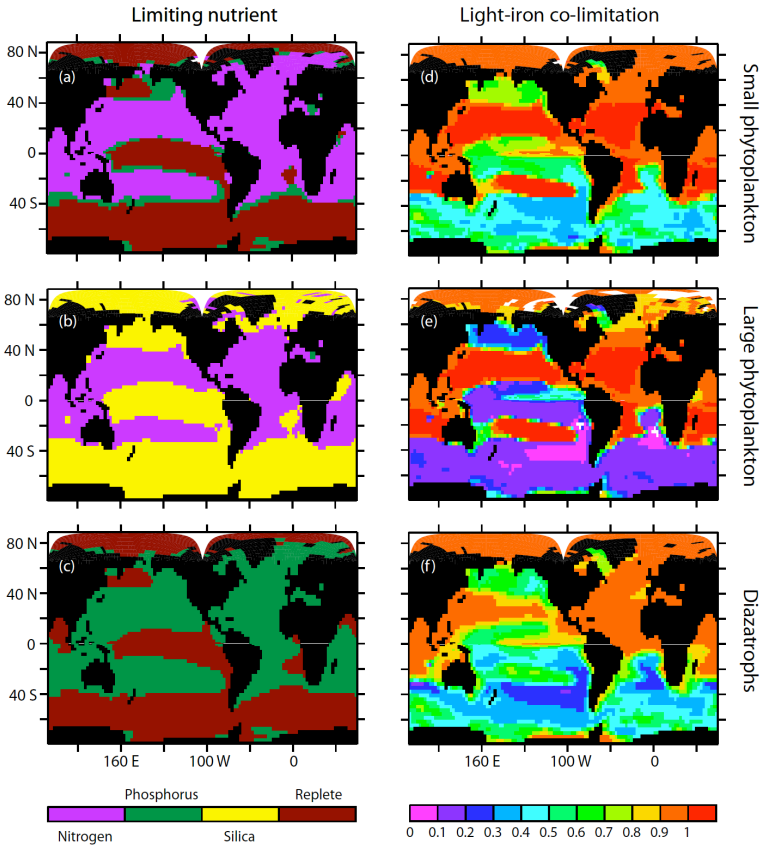

Fig. 1. The left column shows which nutrient is limiting small phytoplankton (top), large phytoplankton (middle), and diazotrophs (bottom). These results are from the control simulation after a 1000 yr spin-up. Replete is defined as minimum limitation ≥0.965. The right column shows the magnitude of the iron-light co-limitation term.

BGD
6, 10381–10446, 2009

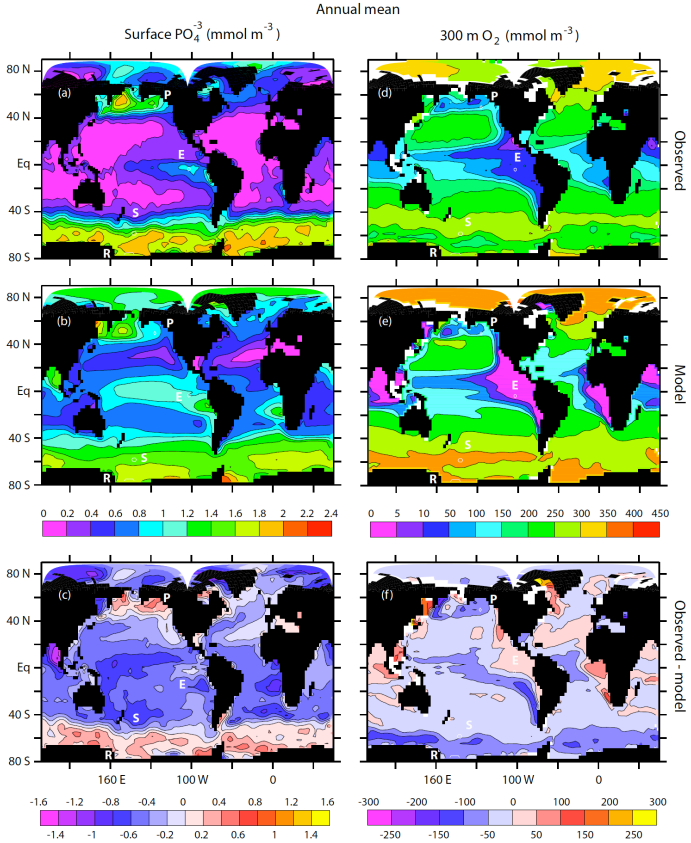

Fig. 2. **(a)** Observed annual mean of the phosphate at the surface of the ocean in mmol m^{-3} (Garcia et al., 2006) compared with **(b)** surface phosphate in the model. **(c)** shows the difference between observed and modeled. **(d)** and **(e)** show the oxygen concentration at 300 m in mmol m^{-3} in the observations and model simulation, respectively, and **(f)** shows the observed minus model oxygen distribution. The figures also show the location of the four iron fertilization sites discussed in the paper. P is the PAPA site, E is the Equatorial Pacific site, S is the Southern Ocean site, and R is the Ross Sea site (see Table 2).

BGD
6, 10381–10446, 2009

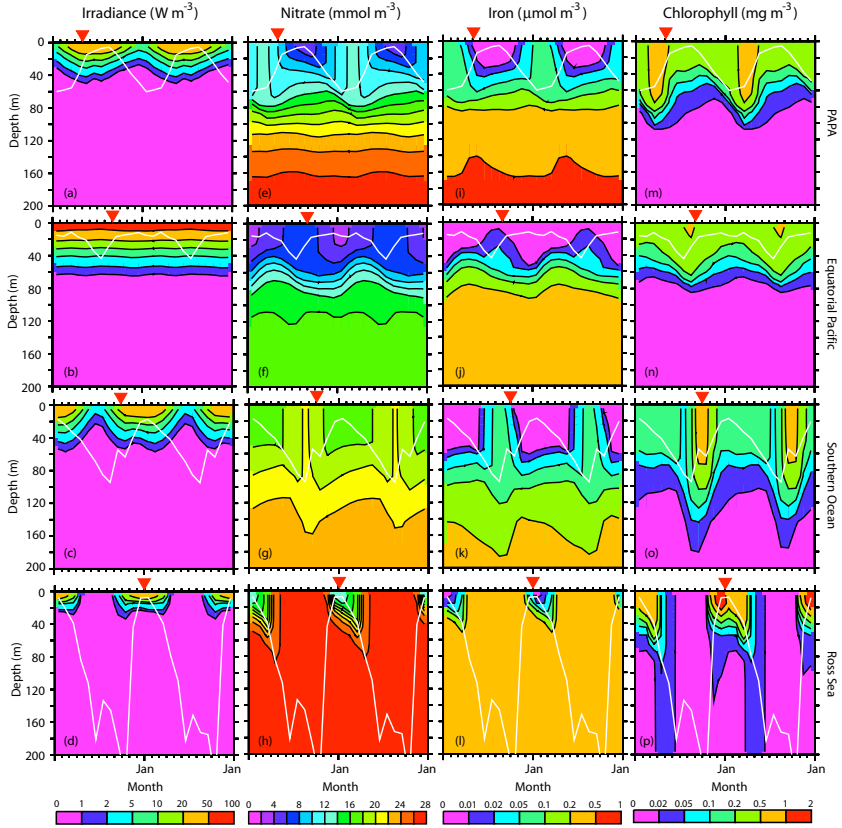

Fig. 3. Results of the control simulation contoured as a function of depth vs. time at each of the four iron fertilization sites. The white line is the KPP mixed layer depth defined in the text. The red arrow at the top is the month when iron is added in the 1×, 10×, and 100× fertilization scenarios. Each row is a separate site with PAPA at the top, the Equatorial Pacific and Southern Ocean in the middle two rows, and the Ross Sea at the bottom. The first column shows irradiance in W m^{-2}, **(a)–(d)**; the second column shows nitrate concentration in mmol m^{-3}, **(e)–(h)**; the third column shows iron concentration in μmol m^{-3}, **(i)–(l)**; and the final column shows chlorophyll concentration in mg m^{-3} **(m)–(p)**. These are all for two years at the start of the control simulation.

BGD
6, 10381–10446, 2009

Efficiency of small scale carbon mitigation by patch iron fertilization

J. L. Sarmiento et al.

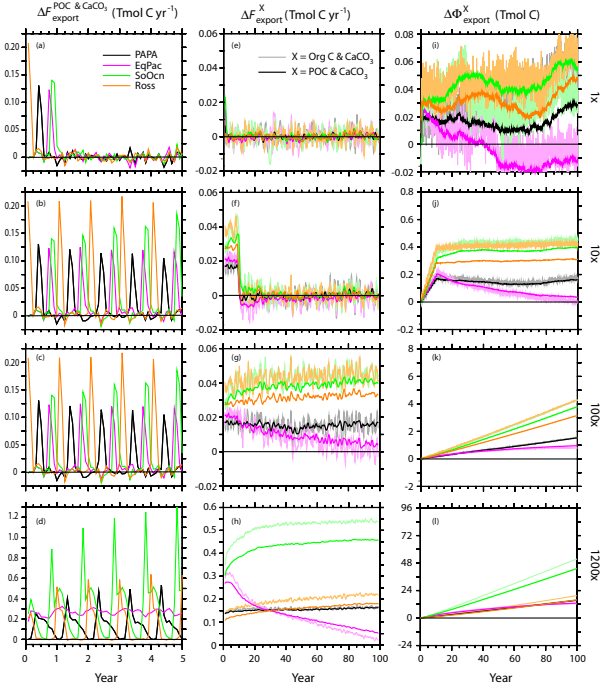

Fig. 4. **(a)**–**(d)** show the perturbation response of the monthly particulate organic carbon (POC) and $CaCO_3$ export production $\Delta F_{export}^{POC\,\&\,CaCO_3}$ over the first 5 yr for better resolution (see Appendix A for a definition of $\Delta F_{export}^{POC\,\&\,CaCO_3}$ and related terms). **(e)**–**(h)** show the monthly carbon export ΔF_{export}^{X} over the first 100 yr. The light colored lines show total carbon, X=Org C & $CaCO_3$, and the dark colored lines show only the particulate component of organic carbon, X=POC & $CaCO_3$. **(i)**–**(l)** show the cumulative export of carbon $\Delta\Phi_{export}^{X}$, with X as above. We define export as the net downward flux across a depth of 98 m. The rows correspond to the 1×, 10×, 100×, and 1200× cases from top to bottom. The flux of dissolved and living organic matter in the Org C component is very noisy, and the total carbon export fluxes in the middle and right hand column were heavily smoothed twice with a 12-month boxcar filter in order to make the different results distinguishable. Note that the POC & $CaCO_3$ export component accounts for most of the export flux at PAPA and the Equatorial Pacific sites, but misses a significant component of the total carbon export at the other two sites.

BGD
6, 10381–10446, 2009

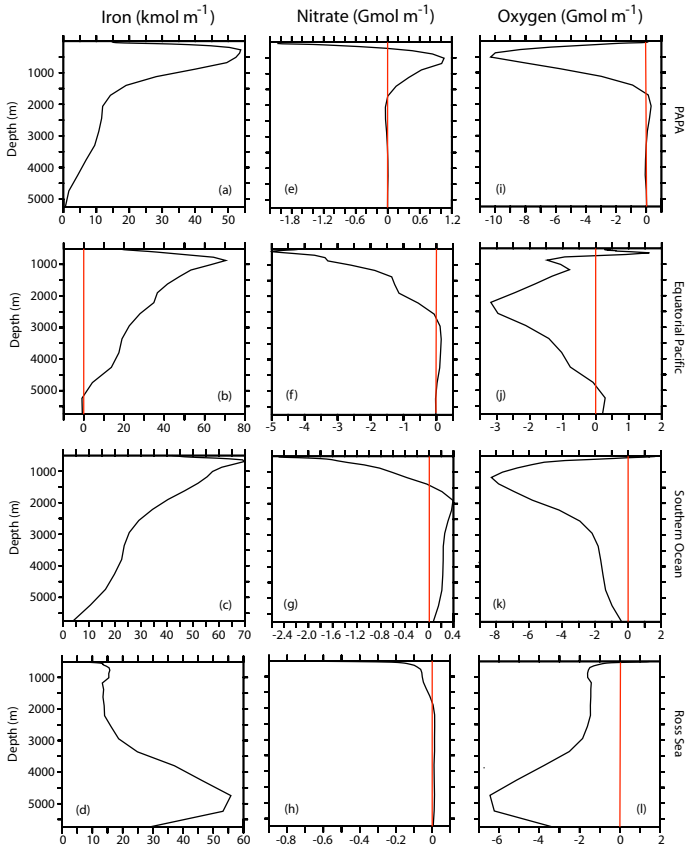

Fig. 5. Global horizontally integrated 100-yr cumulative perturbation results of the 1200× iron fertilization scenarios plotted as a function of depth. The first column, **(a)**–**(d)** is the iron concentration perturbation in kmol m^{-1}; the second column, **(e)**–(**h**) is the nitrate concentration perturbation in Gmol m^{-1}; and the third column, **(i)**–**(l)** is the oxygen concentration perturbation in Gmol m^{-1}. The first row of results is for Papa, the second for the equatorial Pacific, the third for the Southern Ocean and the bottom row is the Ross Sea.

BGD
6, 10381–10446, 2009

Efficiency of small scale carbon mitigation by patch iron fertilization

J. L. Sarmiento et al.

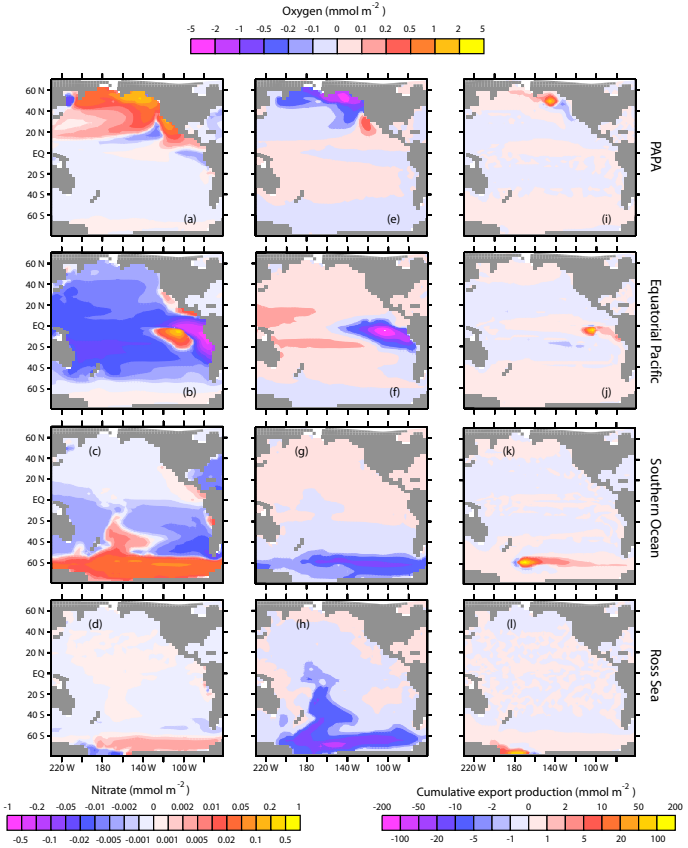

Fig. 6. Perturbation maps of the 1200× iron fertilization scenarios at year 100. The first column, **(a)**–**(d)** shows the nitrate concentration perturbation in mmol m^{-2} integrated vertically from 98 m depth to the bottom; the second column, **(e)**–**(h)** is the oxygen concentration perturbation in mol m^{-2} integrated vertically from 98 m depth to the bottom; and the third column, **(i)**–**(l)** is cumulative export production across 98 m integrated over the 100 yr of the simulation in mmol m^{-2}. The first row of results is for Papa, the second for the equatorial Pacific, the third for the Southern Ocean and the bottom row is the Ross Sea.

BGD
6, 10381–10446, 2009

Efficiency of small scale carbon mitigation by patch iron fertilization

J. L. Sarmiento et al.

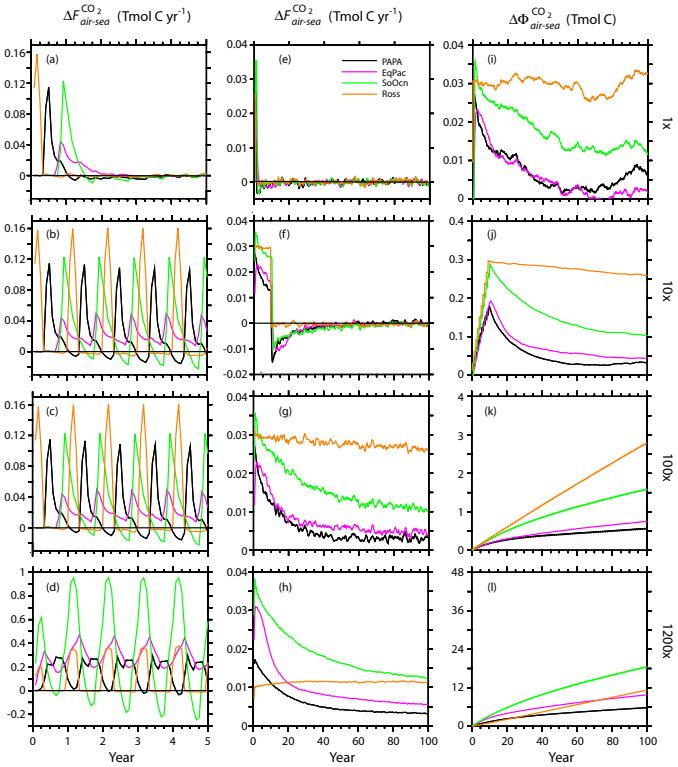

Fig. 7. Results of the iron fertilization scenarios plotted as a function of time for: **(a)–(d)** annual uptake of CO_2 plotted month by month for the first 5 yr, $\Delta F^{CO_2}_{air-sea}$; **(e)**–(**h**) annual uptake of CO_2 from the atmosphere for 100 yr, $\Delta F^{CO_2}_{air-sea}$; **(i)–(l)** cumulative CO_2 uptake from the atmosphere, $\Delta \Phi^{CO_2}_{air-sea}$. The first row of results is for the 1× scenarios, the second for the 10× scenarios, the third for the 100× scenarios, and the bottom row is for the 1200× scenarios.

BGD
6, 10381–10446, 2009

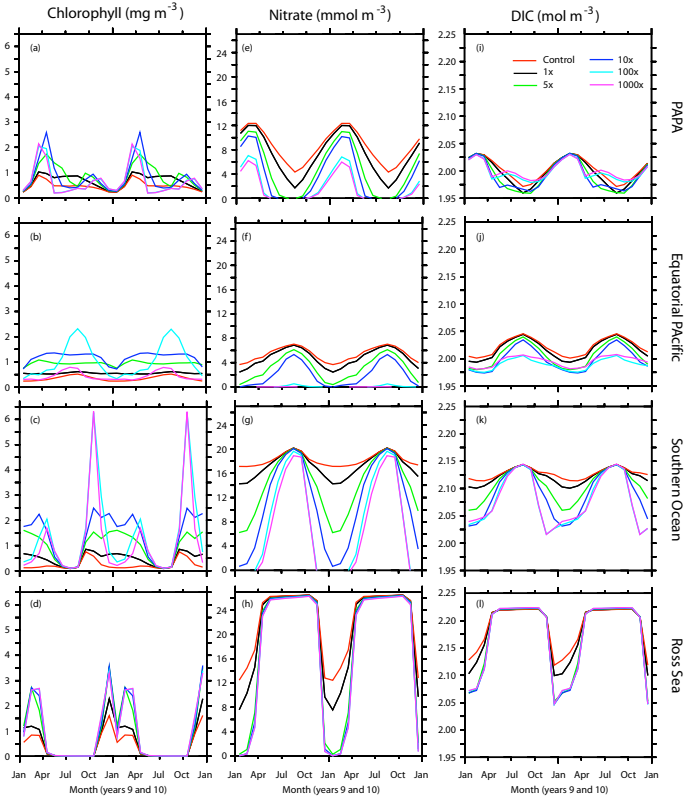

Fig. 8. Mean chlorophyll, nitrate, and DIC in the top 10 m of the four fertilization sites after 10 yr of constant fertilization with increasing additions of iron expressed here as a multiple of the standard IFMIP 1200× scenario. Note that the mean surface nitrate concentration stabilizes after ~4 yr of continuous fertilization so the 10 yr concentration is pretty much already at steady state for the given fertilization scenario.

BGD

6, 10381–10446, 2009

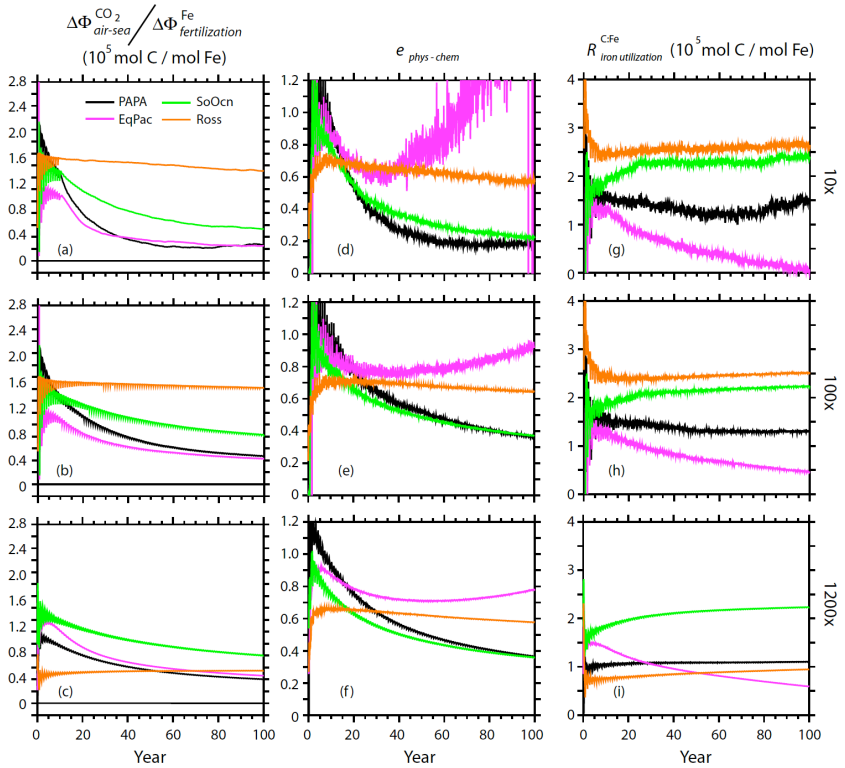

Fig. 9. Results from the iron fertilization scenarios plotted as a function of time from 0 to 100 yr of **(a)–(c)**, the efficiency of CO_2 uptake with respect to iron addition, $R^{C:Fe}_{overall} = \Delta\Phi^{CO_2}_{air-sea} / \Delta\Phi^{Fe}_{fertilization}$, **(d)–(f)** the physical-chemical uptake efficiency $e_{phys-chem}$, and, **(g)–(i)**, the biogeochemical response function, $\Delta R^{C:Fe}_{overall}$. The first row of results is for the 10× scenarios, the second for the 100× scenarios, and the bottom row is for the 1200× scenarios.

BGD
6, 10381–10446, 2009

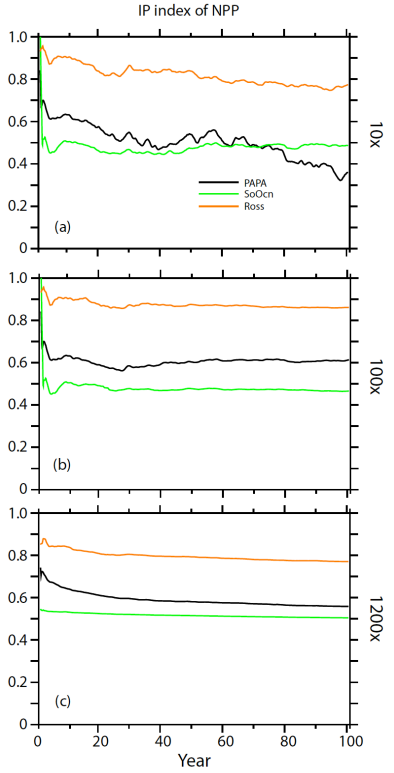

Fig. 10. The fraction of the total perturbation export production across 98 m, $\Delta\Phi_{export}^{OrgC\,\&\,CaCO_3}$, that is due to the perturbation export production in the top box of the model with a thickness of 10 m calculated as a function of time for **(a)** the 10×, **(b)** the 100×, and **(c)** the 1200× scenarios. This is the IP index of Jin et al. (2008). Note that the Ross Sea has the highest index. The Equatorial Pacific site is left off the plot because its trajectory is distorted by the loss of nitrate due to denitrification.

BGD
6, 10381–10446, 2009

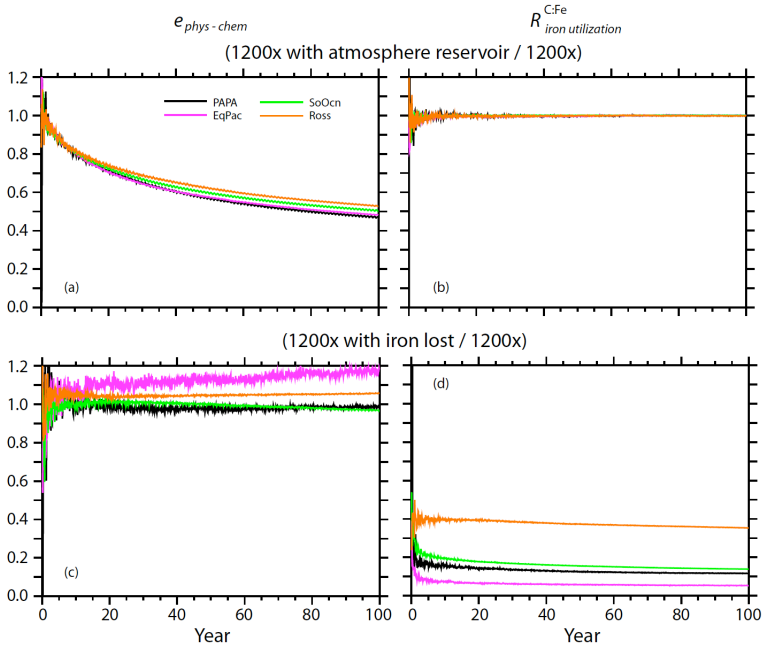

Fig. 11. Sensitivity studies of factors contributing to the efficiency of the 1200× simulations. Panels **(a)** and **(b)** examine the sensitivity to the inclusion of an atmospheric reservoir, and Panels **(c)** and **(d)** examine the sensitivity to the retention of iron, all plotted as a function of time from 0–100 yr. The first row shows the uptake efficiency $e_{\text{phys−chem}}$ and the overall C:Fe iron utilization ratio, $R^{\text{C:Fe}}_{\text{iron addition}}$ for the simulation with a variable atmosphere divided by the corresponding quantity in the standard 1200× simulation. The second row shows $e_{\text{phys−chem}}$ and $R^{\text{C:Fe}}_{\text{iron addition}}$ for the simulation with no iron remineralization divided by the corresponding quantity in the standard 1200× simulation.

BGD
6, 10381–10446, 2009

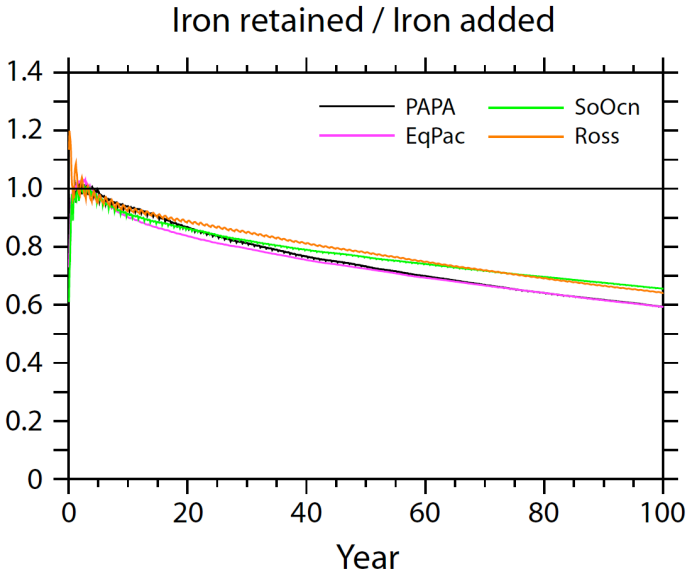

Fig. 12. The ratio of iron retained in the ocean with respect to the iron added in the 1200× scenario. Despite the continuous addition of iron in this model, the scavenging of iron out of the ocean is such that only ~60% of the iron is present at the end of the simulation.

BGD
6, 10381–10446, 2009